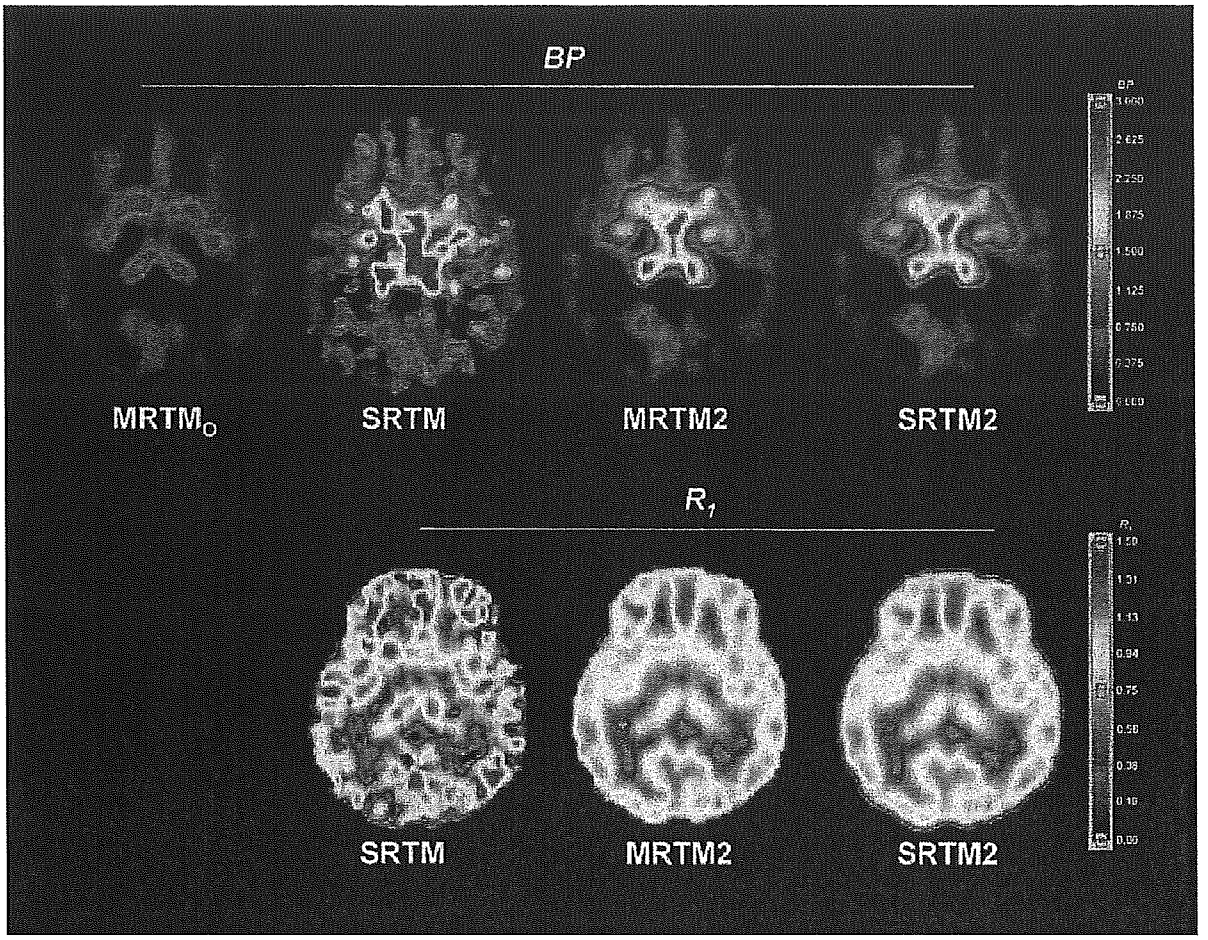

FIG. 8. Parametric images of [^{11}C]DASB *BP* (top row) estimated by MRTM$_O$, SRTM, MRTM2, and SRTM2, and R_1 (bottom row) estimated by SRTM, MRTM2, and SRTM2. *BP*, binding potential; R_1, relative delivery; MRTM$_O$ and MRTM2, original multilinear reference tissue model and its rearranged two-parameter model, respectively; SRTM and SRTM2, simplified reference tissue model and its two-parameter model, respectively.

contained a much greater number of such white matter voxels with high positive *BP* values (Fig. 8).

Fig. 9 shows examples of *BP* and R_1 parametric images estimated by MRTM2 and the corresponding magnetic resonance images from the same subject. In the *BP* images, voxels with corresponding R_1 values below 0.45 were set to 0. In this subject, all of these voxels belonged anatomically to the white matter region on the coregistered magnetic resonance scan (data not shown). This process improved the appearance of white matter regions in the *BP* image by removing the misleading noise-induced high *BP* values. The *BP* images (left column) show that regionally *BP* values are high in the hypothalamus and raphe, moderately high in the thalamus and striatum, and low to very low in the amygdala and cerebral cortex, respectively. This regional *BP* pattern was consistent with the known regional distributions of SERT sites. The R_1 images (middle column) show that R_1 values are high to moderate in the cortex, striatum and thalamus; and relatively low in the hypothalamus, raphe and amygdala, respectively. This regional R_1 pattern was consistent with human imaging studies of cerebral blood flow.

The threshold R_1 value of 0.45 removed 1,800 ± 400 voxels (~70 mL) from the white matter and the resulting *BP* images were visually considered satisfactory in six of eight subjects. There were a few white matter voxels with noise-induced moderately high *BP* in one of the two remaining subjects. In this subject, raising the threshold value to 0.47 removed those misleading voxels. In another subject, the thresholding process produced several sharp edges around the gray matter structures with relatively low flow such as the raphe and hypothalamus, although there were no misleading high-*BP* voxels in the white matter. In this subject, lowering the R_1 threshold value to 0.42 improved the white matter image appearance by removing the sharp edges without reintroducing any visually misleading high-*BP* voxels.

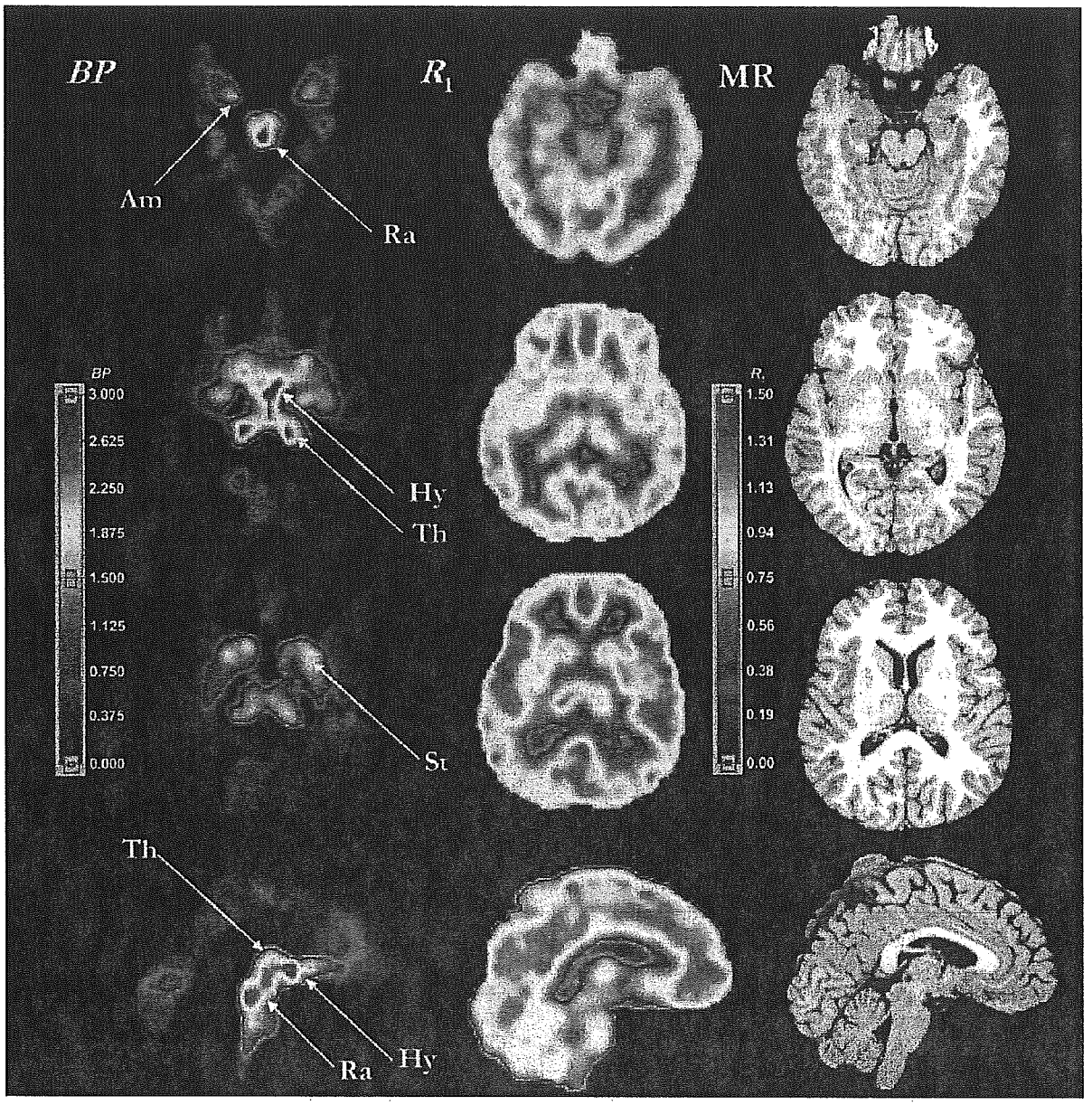

FIG. 9. Parametric images of [^{11}C]DASB *BP* (left column) and R_1 (center column) estimated by MRTM2, and T1-weighted magnetic resonance images (right column). In the *BP* images, all voxels with corresponding R_1 values below 0.45 were set to zero. The top three rows show transverse images and the bottom row shows sagittal images. The *BP* image in the second row corresponds to the MRTM2 *BP* image in Fig. 8. The color display ranges for *BP* and R_1 images are 0 to 3.0 and 0 to 1.50, respectively. Am, amygdala; Hy, hypothalamus; Ra, raphe complex; St, striatum; Th, thalamus; *BP*, binding potential; R_1, relative delivery; MRTM2, two-parameter multilinear reference tissue model.

DISCUSSION

In the present study, we applied two strategies to the original multilinear reference tissue model, $MRTM_O$, to improve parametric images of *BP* and R_1 for human [^{11}C]DASB PET data. First, rearrangement of the $MRTM_O$ operational equation removed a noisy tissue radioactivity term, $C(T)$, from the independent variables, and this MRTM decreased the bias of *BP* estimation substantially, at the expense of considerably increased variability. The three-parameter linear method, MRTM, has similar parameter estimation characteristics to the three-parameter nonlinear method, SRTM (Lammertsma and Hume, 1996). Although this increased *BP* variability with MRTM over $MRTM_O$ did not allow stable *BP* estimations at the voxel level, MRTM did allow estimation

of k_2' with little bias (<1%) and relatively small variability (<6%) from cerebellar and several tissue ROI data. Second, assuming that there is only one k_2' value for the reference region, the number of parameters to estimate was reduced from three in MRTM to two in MRTM2 by using a common value of k_2', in a manner analogous to that used in the nonlinear method SRTM2 (Wu and Carson, 2002). MRTM2 substantially decreased the bias and variability of *BP* and R_1 estimations over the linear and nonlinear three-parameter estimation methods. Furthermore, the linearized approach allowed rapid generation (<15 seconds) of stable parametric images of *BP* in the gray matter and R_1 in the whole brain.

We previously evaluated the effects of the first strategy used here for the estimation of the distribution volume with plasma input function data for two neuroreceptor radioligands, [^{18}F]FCWAY and [^{11}C]MDL 100,907 (Ichise et al, 2002). The resulting linear model (referred to as MA1 in that study) was also nearly identical to its nonlinear counterpart for *V* estimation at the voxel level. Like MRTM2, the operational equation for MA1 has only two parameters to estimate. However, for estimation of *BP* without blood data, an additional parameter appears in the operational equations for both linear and nonlinear reference tissue models, which causes parameter estimation to be less stable under certain circumstances. Therefore, the second strategy of determining a single value for the reference region clearance constant and reducing the number of parameter from three to two was applied for these reference tissue models.

SRTM2 has been developed by Wu and Carson (2002) and evaluated in comparison with SRTM for three radioligands, [^{18}F]FCWAY (5-HT$_{1A}$), [^{11}C]flumazenil (benzodiazepine), and [^{11}C]raclopride (dopamine D$_2$), where the magnitude of improvement in parameter estimation by eliminating one parameter depended on the radioligand's kinetics. In that study, the largest impact of SRTM2 on *BP* estimation was found for [^{11}C]flumazenil, particularly with a 30-minute scan duration, where *BP* variability was reduced from ~10 to ~5% and R_1 variability was reduced by a comparable degree. SRTM2 had a similar pattern of impact for [^{11}C]DASB in the present study, although the magnitude of *BP* noise reduction was even larger.

To understand this behavior, consider the characteristics of the 1T model. Information in the data pertaining to *V* or *BP* is obtained at later times, as each tissue region approaches transient equilibrium with the plasma. Mathematically, this follows the function $[1 - \exp(-k_2 t)]$ as it approaches the value 1. In this framework, ignoring differences in the input function, a 90-minute [^{11}C]DASB scan has kinetically similar characteristics to a 30-minute [^{11}C]flumazenil scan, by having a similar value of $k_2 t$ at the end of the study. For [^{11}C]DASB in the raphe, k_2 = 0.013 min^{-1}, t = 90 minutes, and $k_2 t$ = 1.17, whereas for [^{11}C]flumazenil in the occipital cortex, k_2 = 0.040 min^{-1}, t = 30 minutes, and $k_2 t$ = 1.20. This comparison also clarifies why, for [^{11}C]DASB, the variability of voxel *BP* estimates in the raphe (20%) by SRTM2 or MRTM2 was larger than that in the striatum (12%), where $k_2 t$ = 2.04 (Fig. 1A). This explanation is consistent with the corresponding larger C-R variability values for raphe of 18% compared with 12% for striatum (Table 3). Thus, a [^{11}C]DASB scanning duration of more than 90 minutes may further improve parameter estimation at the voxel level for regions with very high *BP* such as the raphe, although Ginovart et al. (2001) showed that a 90-minute study is probably adequate for ROI-based [^{11}C]DASB analyses.

We used the Cramer-Rao lower bound as a prediction of the minimum possible variance that can be achieved by unbiased estimators. Minimum-variance unbiased estimators are generally desirable, and least-squares estimators usually have these characteristics for linear models (i.e., when the model equations are linear with respect to all the parameters). For nonlinear models, these characteristics are achieved asymptotically (i.e., for low noise). Thus, for nonlinear models, as noise increases, the estimators become biased and the variance diverges from the C-R bound. This can be seen in Table 3 by comparing the *BP* variability values for SRTM and SRTM with their respective C-R values with increasing noise. Note that divergence of the sample variance from the C-R variance occurs at different noise levels depending on the model and the parameter values. For example, at 15% noise for striatum *BP* (Table 3), sample variability for SRTM is dramatically higher than the C-R bound, whereas the SRTM2 sample variability agrees with its theoretical prediction. Also, the R_1 parameter, which appears linearly in the model (Eq. 4), shows an excellent match between sample and C-R variability up to the highest noise levels for SRTM and SRTM2 (Table 4).

From a statistical point of view, the multilinear estimators MRTM$_0$, MRTM, and MRTM2 are not minimum-variance unbiased estimators, because of the use of noisy data *C(T)* in the independent variables (Eqs. 1–3). However, as shown in the Results, the magnitude of bias and variance depends considerably on the structure of the model and the parameter values. MRTM$_0$ produces estimates with large bias and variability smaller than the C-R bound. MRTM generally matches the bias and variance of its nonlinear version, SRTM. However, an interesting estimation condition occurs for MRTM in the frontal cortex. Because of the small *BP* value, there is little difference between the frontal cortex and cerebellum TACs (Fig. 1), and the three-parameter estimation (Eqs. 2 and 4) is unstable. This instability produces different results between the nonlinear SRTM and the linear

MRTM. This can be seen in the higher MRTM *BP* variability compensated by lower MRTM R_1 variability. This effect is due to the high correlation between the first and second independent variables in Eq. 2 for the frontal cortex. Alternatively, MRTM2, while technically not a minimum-variance unbiased estimator, provides identical estimation characteristics for all regions to the corresponding NLS method SRTM2 for [^{11}C]DASB (Tables 3 and 4). It is likely that similar statistical results can be obtained with MRTM2 for other ligands that follow 1T kinetics.

In the simulations, we used a noise-free reference tissue TAC for the reference tissue methods and a noise-free plasma input function for 1TKA. Noise in a reference TAC or plasma input curve would have a global effect on the estimates (i.e., all voxel or ROI estimates for that subject would be affected in a common way). Therefore, this noise would not be reflected in the statistical noise of the image, as estimated in the simulation (Tables 3 and 4, Figs. 2 and 4). Rather, this source of noise would increase intersubject variation and degrade the reproducibility of parameter measurements. In our PET data, the intersubject variability of 1TKA and MRTM2 results were comparable, suggesting that these noise sources are either small or of comparable magnitude.

The simulation results for 1TKA were numerically identical to those of SRTM2 to three significant digits because (1) the operational equation SRTM2 (Eq. 4) is simply a different parameterization of Eq. 5 for 1TKA; (2) for the SRTM2 simulations, the true value of k_2' was used; and (3) for the 1TKA simulations, the true values of K_1' and k_2' were used for calculation of *BP* and R_1. The subtle differences between the two methods were due to slight numerical integration errors of either the reference tissue TAC or plasma TACs. However, for the human PET data, 1TKA and SRTM2 were no longer identical because of the effects of input function measurement errors on 1TKA and differences in k_2' determination between the two methods.

There are a number of technical issues involved in implementing these methods. Both MRTM2 and SRTM2 require accurate *a priori* estimation of k_2'. The simulation results indicated that k_2' estimation by MRTM using a single-tissue ROI such as the striatum has moderate variability (10%) of k_2' estimates, although the bias is very small (<1%). This noise in an individual's k_2' estimate would translate into a bias in all *BP* and R_1 values for that subject (Fig. 6). To reduce this noise, we estimated k_2' values for several tissue ROIs and used a weighted mean of these values for MRTM2 and SRTM2. This strategy reduced the effective variability of k_2' estimates to less than 6%. Alternatively, Wu and Carson (2002) used the median value of estimated by SRTM for all brain voxels with moderate to high *BP*. The use of the median was necessary in their case to avoid bias induced by the noise of each pixel TAC. The median was not required here, using an ROI-based approach for k_2' estimation. Use of the nonlinear SRTM for this purpose can be computationally time consuming, and MRTM could be used instead to improve the processing speed. In any case, the optimal approach for MRTM or SRTM k_2' estimation should be carefully evaluated for each neuroreceptor radioligand of interest.

For the white matter with very low *BP*, voxel-wise *BP* estimation by MRTM2 was somewhat unstable, although MRTM2 reduced white matter noise considerably compared with SRTM (Figs. 5 and 8). To improve the appearance of the white matter in the MRTM2 *BP* image, we used a simple threshold based on a fixed R_1 value. The disadvantage of this approach is that an appropriate threshold R_1 value may differ between subjects (see Results). By increasing the threshold R_1 value, sharp edges appeared around gray matter structures with relatively low blood flow, such as the raphe and hypothalamus, because R_1 values in the neighboring voxels are below the threshold owing to the partial volume effect. An alternative approach to setting *BP* to 0 for R_1 values below a specific cutoff would be to add a constraint to the least-squares fitting, so that parameter estimates are limited to a bounded region in parameter space (Fig. 5). This can be implemented with a two-step procedure, whereby voxels falling outside the permitted space can be refit to find the LS parameter values that fall on the boundary of the permitted space.

To minimize any bias introduced by the integral(s) on the right-hand side of the operational equations (Eqs. 1–4), the sampling rates used in the simulations were twice the rates used in the actual PET data. In addition, the first time point was excluded from fitting. This resulted in bias of no more than 0.1% for all methods in *BP*, R_1, and k_2' estimations with noise-free data (Tables 2–4). Reduction of the sampling rates to those of actual PET data (27 frames) increased the magnitude of bias to approximately 0.3% for all models. Thus, for [^{11}C]DASB, a very high sampling rate is not necessary to avoid integration-induced bias.

In this study, parameter estimation was performed without data weighting. However, MRTM2 (Eq. 3), SRTM2 (Eq. 4), and 1TKA (Eq. 5) can all be applied using weighted least squares estimation to account for noise-level differences in $C(T)$ (Carson, 1986). Using the ideal weights, $1/\mathrm{Var}[C(T)]$, for the current simulated data, weighted least squares improved the bias and variability of *BP* and R_1 estimations by MRTM2 and SRTM2 slightly across all noise levels. For example, the *BP* bias and variability in the raphe by SRTM2 at 15% noise were 2.5% and 16.0% with weighted least squares, and 3.6% and 20.5% unweighted, respectively. Thus, weighted least squares improves parameter estimation

when there is a considerable scan-to-scan variation in noise, as was the case for our 90-minute [^{11}C]DASB PET study with the short half-life of ^{11}C (20.4 minutes) (Fig. 1B).

The two-parameter linear (MRTM2) and nonlinear (SRTM2) models were effectively identical for voxel-wise parameter estimation for these [^{11}C]DASB data. The major advantage of MRTM2 over SRTM2 is the parametric image computation speed, where SRTM2 is more computationally expensive. MRTM2 has another potential advantage over SRTM or SRTM2 in that the linearized models can be applied without assumption of a specific compartment configuration (Logan et al., 1990), as opposed to SRTM or SRTM2 that assume a 1T model for both the reference and tissue regions (Lammertsma et al., 1996). Violations of these compartment model assumptions with SRTM and SRTM2 have been shown to cause biased estimates irrespective of statistical noise in the PET data (Slifstein et al., 2000; Wu and Carson, 2002). However, there are a few issues to be addressed in applying MRTM2 for data that is inconsistent with the 1T model assumptions. First, the parameter R_1 can no longer be estimated accurately, because b in Eq. 3 is not equal to $(-1/k_2)$, but is instead a function of the rate constants k_2, k_3, and k_4 of the 2T model (Ichise et al., 2002; Logan et al., 1990). Second, the fit must be restricted to the "linear" portion of the data (i.e., $t > t^*$, and t^* must be defined). Because the operational equation is asymptotically linear, identification of t^* can be problematic, particularly in the presence of noise in the data (Ichise et al., 2002). Another problem is that t^* may be quite late for 2T radioligands with slow kinetics, resulting in increased statistical noise in the parameter estimates.

Finally, the voxel BP and R_1 values estimated by MRTM2 or SRTM2 without blood data in our eight [^{11}C]DASB PET studies were very similar to those estimated by 1T KA with plasma input function data. Ginovart et al. (2001) have also shown in their ROI-based data analysis that ROI BP values estimated by SRTM correlate well with those by 1TKA for their five human [^{11}C]DASB PET studies. In addition, these investigators have noted that the regional distribution of BP appears to correlate well with the known distribution of the SERT densities in human brain (Ginovart et al., 2001; Houle et al., 2000). The BP parametric images (Figs. 8 and 9) also support these findings. Compared with ROI-based parameter estimations, however, parametric images will allow voxel-based statistical analysis of SERT binding sites throughout the brain, including small structures such as the raphe, hippocampus, and amygdala.

CONCLUSIONS

The two-parameter linearized reference tissue model, MRTM2, which incorporates two strategies to improve parameter estimation at the voxel noise level, allows rapid generation of stable parametric images of binding potential and relative delivery for [^{11}C]DASB PET data. The noise reductions are effectively identical to those of the two-parameter nonlinear reference tissue model, but the computational time is dramatically shortened. This noninvasive MRTM2 should be a useful data analysis tool for [^{11}C]DASB PET studies of the serotonin transporter in human brain.

Acknowledgments: The authors thank Dr. Cyrill Burger for implementing the multilinear reference models in PMOD, Jude Gustafson, M.A., for editing assistance, and the entire PET Department Staff for technical assistance at the National Institute of Radiological Sciences, Chiba, Japan.

REFERENCES

Backstrom I, Bergstrom M, Marcusson J (1989) High affinity [^{3}H]paroxetine binding to serotonin uptake sites in human brain tissue. *Brain Res* 486:261—268

Beck JV, Arnold KJ (1977) *Parametric estimation in engineering science.* New York: John Wiley & Sons, Inc.

Carson RE (1986) Parameter estimation in positron emission tomography. In: *Positron emission tomography. Principles and applications for the brain and the heart* (Phelps ME, Mazziota JC, Schelbert HR, eds), New York: Raven Press, pp 347–390

Carson RE (1993) PET parameter estimation using linear integration methods: bias and variability consideration. In: *Quantification of brain function. Tracer kinetics and image analysis in brain PET* (Uemura K, Lassen NA, Jones T, et al., eds), Amsterdam: Elsevier Science Publishers B.V., pp 81—89

Cortes R, Pazos A, Probst A, Palacios JM (1988) Autoradiography of antidepressant binding sites in the human brain: localization using [^{3}H]imipramine and [^{3}H]paroxetine. *Neuroscience* 27:473—496

Ginovart N, Wilson AA, Meyer JH, Hussey D, Houle S (2001) Positron emission tomography quantification of [^{11}C]DASB binding to the human serotonin transporter: modeling strategies. *J Cereb Blood Flow Metab* 21:1342—1353

Gunn RN, Lammertsma AA, Hume SP, CunninghamVJ (1997) Parametric imaging of ligand-receptor binding in PET using a simplified reference region model. *Neuroimage* 6:279—287

Houle S, Ginovart N, Hussey D, Meyer JH, Wilson AA (2000) Imaging the serotonin transporter with positron emission tomography: initial human studies with [^{11}C]DAPP and [^{11}C]DASB. *Eur J Nucl Med* 27:1719—1722

Huang Y, Hwang D-R, Narendran R, Sudo Y, Chatterjee R, Bae S-A, Mawlawi O, Kegeles LS, Wilson AA, Hank F. Kung HF, Laruelle M (2002) Comparative evaluation in nonhuman primates of five PET radiotracers for imaging the serotonin transporters: [^{11}C]McN 5652, [^{11}C]ADAM, [^{11}C]DASB, [^{11}C]DAPA, and [^{11}C]AFM. *J Cereb Blood Flow Metab* 22:1377—1398

Ichise M, Ballinger JR, Golan H, Vines D, Luong A, Tsai S, Kung HF (1996) Noninvasive quantification of dopamine D2 receptors with iodine-123-IBF SPECT. *J Nucl Med* 37:513—520

Ichise M, Toyama H, Innis RB, Carson RE (2002) Strategies to improve neuroreceptor parameter estimation by linear regression analysis. *J Cereb Blood Flow Metab* 22:1271—1281

Jenkinson M, Bannister P, Brady M, Smith S (2002). Improved optimization for the robust and accurate linear registration and motion correction of brain images. *Neuroimage* 17:825—841.

Lammertsma AA, Bench CJ, Hume SP, Osman S, Gunn K, Brooks DJ, Frackowiak RS (1996) Comparison of methods for analysis of clinical [^{11}C]raclopride studies. *J Cereb Blood Flow Metab* 16:42—52

Lammertsma AA, Hume SP (1996) Simplified reference tissue model for PET receptor studies. *Neuroimage* 4:153—158

Lesch KP (1997) Molecular biology, pharmacology, and genetics of the serotonin transporter: psychobiological and clinical implications.

In: *Handbook of experimental pharmacology. Serotoninergic neurons and 5-HT receptors in the CNS* (Baumgarten HG, Gothert M, eds), Berlin: Springer-Verlag, pp 671—705

Logan J, Fowler JS, Volkow ND, Wolf AP, Dewey SL, Schlyer DJ, MacGregor RR, Hitzemann R, Bendriem B, Gatley SJ (1990) Graphical analysis of reversible radioligand binding from time-activity measurements applied to [*N*-^{11}C-methyl]-(−)-cocaine PET studies in human subjects. *J Cereb Blood Flow Metab* 10:740—747

Logan J, Fowler JS, Volkow ND, Wang GJ, Ding YS, Alexoff DL (1996) Distribution volume ratios without blood sampling from graphical analysis of PET data. *J Cereb Blood Flow Metab* 16:834—840

Logan J, Fowler JS, Volkow ND, Ding YS, Wang GJ, Alexoff DL (2001) A strategy for removing the bias in the graphical analysis method. *J Cereb Blood Flow Metab* 21:307—320

Lopez-Ibor JJ Jr (1988) The involvement of serotonin in psychiatric disorders and behavior. *Br J Psychiatry* 3(Suppl):26—39

Mikolajczyk K, Szabatin M, Rudnicki P, Grodzki M, Burger C (1998) A JAVA environment for medical image data analysis: initial application for brain PET quantitation. *Med Inform* 23:207—14

Mintun MA, Raichle ME, Kilbourn MR, Wooten GF, Welch MJ (1984) A quantitative model for the *in vivo* assessment of drug binding sites with positron emission tomography *Ann Neurol* 15:217—227

Rosel P, Menchon JM, Oros M, Vallejo J, Cortadellas T, Arranz B, Alvarez P, Navarro MA (1997) Regional distribution of specific high affinity binding sites for ^{3}H-imipramine and ^{3}H-paroxetine in human brain. *J Neural Transm* 104:89—96

Slifstein M, Laruelle M (2000) Effects of statistical noise on graphic analysis of PET neuroreceptor studies. *J Nucl Med* 41:2083—2088

Slifstein M, Parsey RV, Laruelle M (2000) Derivation of [11C]WAY 100635 binding parameters with reference tissue models: effect of violations of model assumptions. *Nucl Med Biol* 27:487—492

Varga J, Szabo Z (2002) Modified regression model for the Logan plot. *J Cereb Blood Flow Metab* 22:2

Wilson AA, Ginovart N, Schmidt M, Meyer JH, Threlkeld PG, Houle S (2000a) Novel radiotracers for imaging the serotonin transporter by positron emission tomography: synthesis, radiosynthesis, and *in vitro* and ex vivo evaluation of ^{11}C-labeled 2-(phenylthio)araalkylamines. *J Med Chem* 43:3103—3110

Wilson AA, Garcia A, Jin L, Houle S (2000b) Radiotracer synthesis from [^{11}C]-iodomethane: a remarkably simple captive solvent method. *Nucl Med Biol* 27:529—532

Wilson AA, Ginovart N, Hussey D, Meyer J, Houle S (2002) In vitro and *in vivo* characterisation of [^{11}C]DASB: a probe for *in vivo* measurements of the serotonin transporter by positron emission tomography. *Nucl Med Biol* 29:509—515

Wu Y, Carson RE (2002) Noise reduction in the simplified reference tissue model for neuroreceptor functional imaging. *J Cereb Blood Flow Metab* 22:1440—1452

ELSEVIER

Neuroscience Letters 336 (2003) 171–174

Neuroscience Letters

www.elsevier.com/locate/neulet

Different roles of group I and group II metabotropic glutamate receptors on phencyclidine-induced dopamine release in the rat prefrontal cortex

Jun Maeda[a,b,c], Tetsuya Suhara[a,b,*], Takashi Okauchi[a,b,c], Jun'ichi Semba[b,d]

[a]*Brain Imaging Project, National Institute of Radiological Sciences, 9-1, Anagawa 4-Chome, Inage-ku, Chiba, Japan*
[b]*CREST, Japan Science and Technology Corporation (JST), Saitama, Japan*
[c]*SHI Accelerator Service LTD., Tokyo, Japan*
[d]*Division of Health Sciences, University of the Air, Chiba, Japan*

Received 5 June 2002; received in revised form 25 October 2002; accepted 26 October 2002

Abstract

The dopamine system in the limbic-prefrontal cortex has been assumed to play an important role in the cognitive dysfunction of schizophrenia and phencyclidine (PCP)-induced psychosis. In the present study, the role of metabotropic glutamate (mGlu) receptor subtypes on PCP-induced cortical dopamine release was investigated using the microdialysis technique. Infusion of 50 and 100 μM of non-selective mGlu receptor agonist trans-(1S,3R)-1-amino-1,3-cyclopentanedicarboxylic acid inhibited PCP-induced dopamine release, while the basal dopamine level was not significantly affected. A similar inhibition of PCP-induced dopamine release was observed with 100 and 500 μM of selective group I mGlu receptor agonist, (+)-3-hydroxy-phenylglycine. On the other hand, infusion of 10 μM of selective group II mGlu receptor agonist, 2-(2, 3-dicarboxycyclopropyl)-glycine, enhanced the PCP-induced dopamine increase. These results suggest that group I and II mGlu receptors exert opposite modulations on the PCP-induced dopamine release.

Keywords: Phencyclidine; Metabotropic glutamate receptor; Prefrontal cortex; Dopamine; Microdialysis

Phencyclidine (PCP) is known to cause hallucinations and cognitive dysfunction in humans [8]. PCP has noncompetitive *N*-methyl-D-aspartate (NMDA) receptor antagonistic properties [8]. It is reported to exacerbate symptoms of schizophrenia, and its acute or repeated administration can also produce abnormal motor behavior and cognitive impairments in rats and monkeys [1,8,9,11,12]. Since acute PCP treatment produces dysfunctions in the mesocortical dopaminergic and glutamatergic systems, it may be related to the pathophysiology of PCP-psychosis and symptoms of schizophrenia [8,12].

Glutamate receptors are largely classified into ionotropic and metabotropic types. The metabotropic glutamate (mGlu) receptors can be divided into eight subtypes. These subtypes are classified into three groups – group I (mGlu 1,5), which activates inositol 1,4,5-triphosphate (IP_3) metabolic turnover, and groups II (mGlu 2,3) and III (mGlu 4, 6, 7, 8), which inhibit cAMP production [19]. The mGlu receptors are abundantly distributed in the limbic region and prefrontal cortex, and they are suggested to regulate dopamine release [21]. A recent report indicated that the use of mGlu receptor agonists improves the PCP-induced dysfunction of working memory [12]. However, the exact action of mGlu receptors underlying the PCP-induced dopamine release in the cortical region is not yet clear. The purpose of this study is to examine the role of mGlu receptors in the PCP-induced dopamine increase in the prefrontal cortex.

Male Sprague–Dawley rats (Clea Japan Inc., Japan) weighing 180–200 g were housed three or four per cage at a constant room temperature (25 °C) under a 12/12 h light/dark cycle (light: 07:00–19:00) for 2–4 weeks. The procedures performed in this study were approved by the Ethics and Animal Experiments Committee of the National Institute Radiological Sciences, Chiba, Japan. The rats were anesthetized with sodium pentobarbital (60 mg/kg, i.p.), and then placed in a stereotactic apparatus. A guide cannula of 8 mm length (Eicom Corporation, Japan) was surgically

* Corresponding author. Tel.: +81-43-206-3251; fax: +81-43-253-0396.
E-mail address: suhara@nirs.go.jp (T. Suhara).

0304-3940/02/$ - see front matter © 2002 Elsevier Science Ireland Ltd. All rights reserved.
doi:10.1016/S0304-3940(02)01261-2

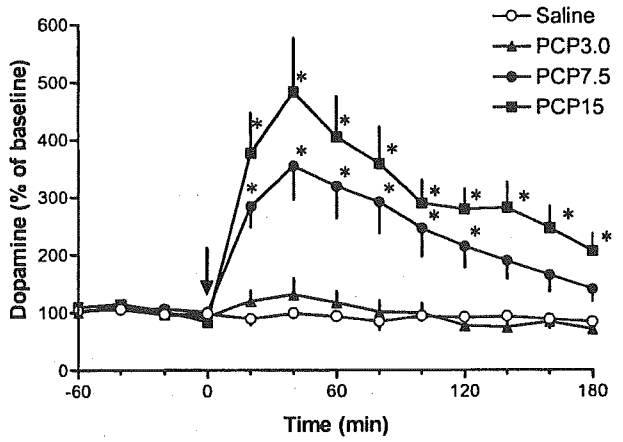

Fig. 1. Dose-dependent increase of dopamine by PCP (3.0–15 mg/kg, i.p.) in the frontal cortex. The arrow indicates the time point of PCP injection. Each point represents the mean ± SEM ($n = 4$–8). *$P < 0.05$ vs. saline-treated controls.

implanted into the prefrontal cortex (coordinates A +2.5 mm, L +0.6 mm, V −3.0 mm from bregma) with reference to a brain atlas [13]. The rats were allowed to recover for at least 2 days before the infusion experiments.

On the day of the infusion, a microdialysis probe (membrane length 3.0 mm, Eicom Corporation, Japan) was inserted with the guide cannula under light anesthesia with diethyl ether, and the guide cannula was fixed with a screw. The probe was perfused with 2.0 μl/min of Ringer's solution (147 mM Na^+, 4 mM K^+, 2.3 mM Ca^{2+}, 155.6 mM Cl^-). The outflow from the prefrontal cortex was collected with a fraction collector and sampling was started 2 h after the start of infusion at 20 min intervals. At first, PCP (3–15 mg/kg, i.p.) was administered to evaluate the effect on basal dopamine release. Then, the effect of mGlu receptor agonists on PCP-induced dopamine release was investigated. The infusion of mGlu receptor agonist was started after collecting three fractions. One hour after the start of the infusion, the rats were treated with PCP (7.5 mg/kg, i.p.), and the infusion was terminated 1 h after the treatment. The dialysates were automatically injected into a high pressure liquid chromatography-electrochemical detector system with reverse-phase column (Eicom Corporation, Japan). We used 0.1 M sodium acetate–citrate buffer (10:7, pH 3.5), 180 mg/l sodium octane sulfonate, 10 mg/l EDTA2Na and 15–17% methanol as a mobile phase (flow rate 0.23 ml/min). Chromatography data were calculated according to the peak area under the dopamine curve. PCP was kindly provided by Yamanouchi Pharmaceutical Co. Ltd. (Japan). Trans-(1S,3R)-1-amino-1,3-cyclopentanedicarboxylic acid (ACPD) and (+)-3-hydroxyphenylglycine (3-HPG) were purchased from Sigma-RBI (USA). (2S,1′R,2′R,3′R)-2-(2′,3′-dicarboxycyclopropyl)-glycine (DCG-IV) was purchased from Tocris Cookson Ltd. (UK). The doses of the mGlu agonists were chosen according to previous microdialysis studies [2,5,16,20,23]. There were no reports about 3-HPG. However, as 3-HPG has weaker potency than 3,5-DHPG with similar selectivity [19], we selected doses of 100 and 500 μM, based on experiments using 3,5-DHPG [16]. All values were expressed as percentage of the baseline level. The effects of mGlu receptor agonists on the basal and PCP-induced dopamine releases between doses and time were evaluated by two-way analysis of variance with repeated measures. When there was a statistically significant difference ($P < 0.05$), post-hoc analysis by Bonferroni–Dunn's test was performed.

The basal concentration of extracellular dopamine in the prefrontal cortex was 0.40 ± 0.04 fmol/μl (mean ± SEM.; $n = 96$). Fig. 1 illustrates that PCP (3.0–15 mg/kg, i.p.) increased dopamine release in the prefrontal cortex in a dose-dependent manner [dose × time; $F_{(9,162)} = 4.69$, $P < 0.001$]. Dopamine release was increased by 3.5- and 4.8-fold after injections of 7.5 and 15 mg/kg of PCP, respectively. In case the PCP-induced dopamine release might be enhanced by mGlu receptor agonists, we chose the lower dose of 7.5 mg/kg to evaluate their effect. Fig. 2 shows the effect of a non-selective mGlu receptor agonist, ACPD, on the PCP-induced dopamine release in the prefrontal cortex. Infusion of 50 and 100 μM of ACPD via dialysis probe inhibited the PCP (7.5 mg/kg, i.p.)-induced dopamine release [dose × time; $F_{(9,162)} = 2.10$, $P < 0.01$], while the basal dopamine level was not significantly affected [dose × time; $F_{(3,54)} = 0.63$, $P > 0.1$]. Fig. 3A shows the effect of a selective group I mGlu receptor agonist, 3-HPG, on the PCP (7.5 mg/kg, i.p.)-induced dopamine release in the prefrontal cortex. The local application of 3-HPG (100 and 500 μM) also inhibited PCP-induced dopamine release [dose × time; $F_{(9,153)=}2.85$, $P < 0.001$] without a notable effect on the basal release [dose × time; $F_{(3,51)} = 1.91$, $P > 0.05$]. Fig. 3B shows the effect of a selective group II mGlu receptor agonist, DCG-IV, on the PCP (7.5 mg/kg, i.p.)-induced dopamine release in the prefrontal cortex. Infusion of 10 μM of DCG-IV significantly potentiated PCP-increased

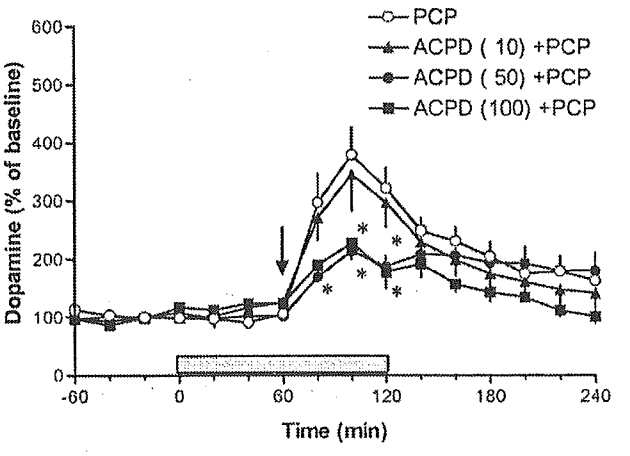

Fig. 2. Effect of non-selective mGlu receptor agonist, 1S, 3R-ACPD (10–100 μM), on PCP-induced dopamine release. The horizontal solid bar indicates infusion of 1S, 3R-ACPD, and the arrow indicates the injection of PCP. Each point represents the mean ± SEM ($n = 4$–8). *$P < 0.05$ vs. PCP-treated controls.

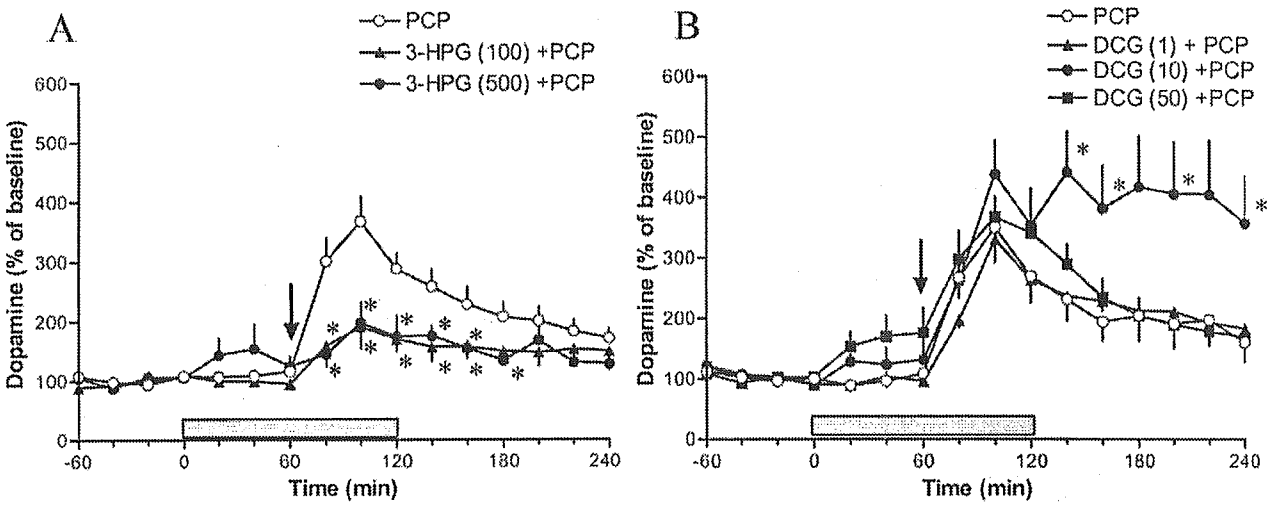

Fig. 3. (A) Effects of selective group I mGlu receptor agonist, 3-HPG (100 and 500 μM), on PCP-induced dopamine release. The horizontal solid bar indicates infusion of each 3-HPG and the arrow indicates the injection of PCP. (B) Effects of selective group II mGlu receptor agonist, DCG-IV (1, 10 and 50 μM), on PCP-induced dopamine release. The horizontal solid bar indicates infusion of each DCG-IV and the arrow indicates the injection of PCP. Each point represents the mean ± SEM ($n = 6$–9). *$P < 0.05$ vs. PCP-treated controls.

dopamine release [dose × time; $F_{(9,243)} = 2.58$, $P < 0.001$]. DCG-IV also slightly, but not significantly, enhanced the basal dopamine release [dose × time; $F_{(3,81)} = 1.30$, $P > 0.1$]. In our previous study, recovery by the microdialysis probe was estimated to be about 10–20% [10].

The main findings of the present work were that the mGlu receptors modulated the PCP-induced dopamine release in the rat prefrontal cortex and that the modulation of mGlu receptor agonist on the dopamine release was different between group I and II subtypes. We demonstrated that the infusion of 50 and 100 μM of ACPD (non-selective mGlu receptor agonist) into the prefrontal cortex inhibited the PCP-induced dopamine release. A similar inhibitory effect was also observed by perfusing the group I selective agonist 3-HPG. These results suggest that ACPD can inhibit PCP-induced dopamine increase via group I mGlu receptors. Previous studies reported that excessive dopamine release by high K^+ stimulation [23], stress induction [5] and cortical electrical stimulation [20] was also inhibited by ACPD in the striatum or medial frontal cortex. Since both agonists per se fail to decrease basal dopamine release (Figs. 2 and 3A), it seems that these inhibitions of PCP-induced dopamine release produced by ACPD and 3-HPG are mediated by indirect regulation of the dopaminergic system. In fact, an immunohistochemical study showed a lack of $mGlu_1$ receptors on dopamine nerve terminals [22]. On the other hand, group I mGlu receptors locate on γ-aminobutyric acid (GABA) neurons [17,22], and their activation could promote GABA release [4]. Previous reports have suggested that endogenous GABA in the prefrontal cortex tonically inhibits dopamine release [18]. PCP decreases GABA release through the antagonism of NMDA receptors on GABA neurons and subsequently increases dopamine release [6,24]. It can be assumed that the stimulation of group I mGlu receptors counteracts the decline of GABA release induced by PCP. Furthermore, the activation of group I mGlu receptors can stimulate glutamate and adenosine release [4,15,16]. The increase in glutamate and other neurotransmitters might be integrated in the regulation of PCP-induced dopamine release.

The infusion of 10 μM of group II agonist DCG-IV enhanced the PCP-induced dopamine release in our study (Fig. 3B). Moreover, DCG-IV also slightly increased basal dopamine release. Moghaddam and Adams [12] reported that there was very slight enhancement in PCP-induced cortical dopamine release by a certain dose of another group II mGlu agonist, LY354740 (10 mg/kg, i.p.). This difference can be explained by drug potency and doses. In fact, Cartmell et al. [3] reported that yet another mGlu agonist, LY379268 (0.3–3 mg/kg, s.c.), with 8-fold higher potency than LY354740, increased basal dopamine release in the prefrontal cortex. The present study showed that there was a significant enhancement of PCP-induced dopamine release at 10 μM of DCG-IV infusion but not at 1 or 50 μM. It has been reported that group II mGlu receptors locate both on glutamatergic and GABAergic neurons [14,22], and their stimulations were reported to decrease the release of glutamate and GABA [4]. The activation of group II mGlu receptor seems to modulate dopamine release indirectly through both excitatory and inhibitory amino acid systems. Furthermore, the selectivity of DCG-IV can also explain the present result. Since it has 10-fold lower affinity to NMDA receptors than group II mGlu receptors [7,19] and the activation of NMDA receptors attenuates PCP-induced dopamine release [24], an inhibition effect may be expected with a relatively high dose of DCG-IV.

In conclusion, the selective group I mGlu receptor agonist 3-HPG inhibited PCP-induced dopamine release in the

prefrontal cortex, while selective group II receptor agonist DCG-IV enhanced PCP-induced dopamine release in the prefrontal cortex. These results suggest that both mGlu receptors can regulate dopamine release, but in an opposite manner, in the prefrontal cortex.

[1] Adams, B. and Moghaddam, B., Corticolimbic dopamine neurotransmission is temporally dissociated from the cognitive and locomotor effects of phencyclidine, J. Neurosci., 18 (1998) 5545–5554.
[2] Bruton, R.K., Ge, J. and Barnes, N.M., Group I mGlu receptor modulation of dopamine release in the rat striatum in vivo, Eur. J. Pharmacol., 369 (1999) 175–181.
[3] Cartmell, J., Perry, K.W., Salhoff, C.R., Monn, J.A. and Schoepp, D.D., The potent, selective mGlu2/3 receptor agonist LY379268 increases extracellular levels of dopamine, 3,4-dihydroxyphenylacetic acid, homovanillic acid, and 5-hydroxyindole-3-acetic acid in the medial prefrontal cortex of the freely moving rat, J. Neurochem., 75 (2000) 1147–1154.
[4] Cartmell, J. and Schoepp, D.D., Regulation of neurotransmitter release by metabotropic glutamate receptors, J. Neurochem., 75 (2000) 889–907.
[5] Feenstra, M.G., Botterblom, M.H. and van Uum, J.F., Local activation of metabotropic glutamate receptors inhibits the handling-induced increased release of dopamine in the nucleus accumbens but not that of dopamine or noradrenaline in the prefrontal cortex: comparison with inhibition of ionotropic receptors, J. Neurochem., 70 (1998) 1104–1113.
[6] Hondo, H., Nakahara, T., Nakamura, K., Hirano, M., Uchimura, H. and Tashiro, N., The effect of phencyclidine on the basal and high potassium evoked extracellular GABA levels in the striatum of freely-moving rats: an in vivo microdialysis study, Brain Res., 671 (1995) 54–62.
[7] Hu, G., Duffy, P., Swanson, C., Ghasemzadeh, M.B. and Kalivas, P.W., The regulation of dopamine transmission by metabotropic glutamate receptors, J. Pharmacol. Exp. Ther., 289 (1999) 412–416.
[8] Javitt, D.C. and Zukin, S.R., Recent advances in the phencyclidine model of schizophrenia, Am. J. Psychiatry, 148 (1991) 1301–1308.
[9] Jentsch, J.D., Redmond Jr, D.E., Elsworth, J.D., Taylor, J.R., Youngren, K.D. and Roth, R.H., Enduring cognitive deficits and cortical dopamine dysfunction in monkeys after long-term administration of phencyclidine, Science, 277 (1997) 953–955.
[10] Maeda, J., Suhara, T., Ogawa, M., Okauchi, T., Kawabe, K., Zhang, M.-R., Semba, J. and Suzuki, K., In vivo binding properties of [carbonyl-^{11}C]WAY-100635: effect of endogenous serotonin, Synapse, 40 (2001) 122–129.
[11] McCullough, L.D. and Salamone, J.D., Increases in extracellular dopamine levels and locomotor activity after direct infusion of phencyclidine into the nucleus accumbens, Brain Res., 577 (1992) 1–9.
[12] Moghaddam, B. and Adams, B.W., Reversal of phencyclidine effects by a group II metabotropic glutamate receptor agonist in rats, Science, 281 (1998) 1349–1352.
[13] Paxinos, G. and Watson, C., The Rat Brain in Stereotaxic Coordinates, 4th Edition, Academic Press, San Diego, CA, 1998.
[14] Petralia, R.S., Wang, Y.X., Niedzielski, A.S. and Wenthold, R.J., The metabotropic glutamate receptors, mGluR2 and mGluR3, show unique postsynaptic, presynaptic and glial localizations, Neuroscience, 71 (1996) 949–976.
[15] Pintor, A., Pezzola, A., Reggio, R., Quarta, D. and Popoli, P., The mGlu5 receptor agonist CHPG stimulates striatal glutamate release: possible involvement of A_{2A} receptors, NeuroReport, 11 (2000) 3611–3614.
[16] Pintor, A., Potenza, R.L., Domenici, M.R., Tiburzi, F., Reggio, R., Pezzola, A. and Popoli, P., Age-related decline in the functional response of striatal group I mGlu receptors, NeuroReport, 11 (2000) 3033–3038.
[17] Romano, C., Sesma, M.A., McDonald, C.T., O'Malley, K., van den Pol, A.N. and Olney, J.W., Distribution of metabotropic glutamate receptor mGluR5 immunoreactivity in rat brain, J. Comp. Neurol., 355 (1995) 455–469.
[18] Santiago, M., Machado, A. and Cano, J., Regulation of the prefrontal cortical dopamine release by $GABA_A$ and $GABA_B$ receptor agonists and antagonists, Brain Res., 630 (1993) 28–31.
[19] Schoepp, D.D., Jane, D.E. and Monn, J.A., Pharmacological agents acting at subtypes of metabotropic glutamate receptors, Neuropharmacology, 38 (1999) 1431–1476.
[20] Taber, M.T. and Fibiger, H.C., Electrical stimulation of the prefrontal cortex increases dopamine release in the nucleus accumbens of the rat: modulation by metabotropic glutamate receptors, J. Neurosci., 15 (1995) 3896–3904.
[21] Testa, C.M., Standaert, D.G., Young, A.B. and Penney Jr, J.B., Metabotropic glutamate receptor mRNA expression in the basal ganglia of the rat, J. Neurosci., 14 (1994) 3005–3018.
[22] Testa, C.M., Friberg, I.K., Weiss, S.W. and Standaert, D.G., Immunohistochemical localization of metabotropic glutamate receptors mGluR1a and mGluR2/3 in the rat basal ganglia, J. Comp. Neurol., 390 (1998) 5–19.
[23] Verma, A. and Moghaddam, B., Regulation of striatal dopamine release by metabotropic glutamate receptors, Synapse, 28 (1998) 220–226.
[24] Yonezawa, Y., Kuroki, T., Kawahara, T., Tashiro, N. and Uchimura, H., Involvement of gamma-aminobutyric acid neurotransmission in phencyclidine-induced dopamine release in the medial prefrontal cortex, Eur. J. Pharmacol., 341 (1998) 45–56.

Pergamon

SCIENCE DIRECT®

Bioorganic & Medicinal Chemistry Letters 13 (2003) 201–204

BIOORGANIC & MEDICINAL CHEMISTRY LETTERS

[^{18}F]FMDAA1106 and [^{18}F]FEDAA1106: Two Positron-Emitter Labeled Ligands for Peripheral Benzodiazepine Receptor (PBR)

Ming-Rong Zhang,[a,b,*] Jun Maeda,[a,b] Kenji Furutsuka,[a,b] Yuichiro Yoshida,[a,b] Masanao Ogawa,[a,b] Tetsuya Suhara[a,c] and Kazutoshi Suzuki[a]

[a]*Department of Medical Imaging, National Institute of Radiological Sciences, 4-9-1 Anagawa, Inage-ku, Chiba 263-8555, Japan*
[b]*SHI Accelerator Service Co. Ltd., 5-9-11 Kitashinagawa, Shinagawa-ku, Tokyo 141-8686, Japan*
[c]*CREST, Japan Sciences and Technology Corporation, 4-1-8 Honmachi, Kawaguchi 332-0012, Japan*

Received 2 September 2002; accepted 12 October 2002

Abstract—We synthesized and evaluated *N*-(5-fluoro-2-phenoxyphenyl)-*N*-(2-[^{18}F]fluoromethyl-5-methoxybenzyl)acetamide ([^{18}F]-FMDAA1106) and *N*-(5-fluoro-2-phenoxyphenyl)-*N*-(2-[^{18}F]fluoroethyl-5-methoxybenzyl)acetamide ([^{18}F]FEDAA1106) as two potent radioligands for peripheral benzodiazepine receptors (PBR). [^{18}F]FMDAA1106 and [^{18}F]FEDAA1106 were respectively synthesized by fluoroalkylation of the desmethyl precursor DAA1123 with [^{18}F]FCH_2I and [^{18}F]FCH_2CH_2Br. Ex vivo autoradiograms of [^{18}F]FMDAA1106 and [^{18}F]FEDAA1106 binding sites in the rat brains revealed that a high radioactivity was present in the olfactory bulb, the highest PBR density region in the brain.

Benzodiazepine receptors are divided into two types: central and peripheral benzodiazepine receptors. Although peripheral benzodiazepine receptor (PBR) was initially identified in the peripheral system, it became clear that its density in the brain regions can equal or exceed the density of central benzodiazepine receptor (CBR) in the corresponding regions.[1–3] Recent studies have shown that PBR might mediate physiological responses in the central nervous system and may be involved in certain pathophysiological events, such as anxiety, by stimulating the production of neuroactive steroids in glial cells in the brain.[4,5] Therefore, the PBR ligands may become effective anxiolytics without the side effects sometimes seen with classical benzodiazepines.[3,5] However, in contrast to the clarification of CBR at the molecular level, the pharmacological characterization of PBR in primate brain has not been fully elucidated.[3,4] Moreover, the precise physiological significance of events mediated through PBR in the brain and the therapeutic potential of PBR antagonists in the pathology and/or etiology of central nervous system disorders are still subjects of controversy.[3–5] As a result there has been great interest in developing radioligands that could be used to visualize the distribution of PBR in a living human brain using positron emission tomography (PET).[6,7]

Recently, *N*-(2,5-dimethoxybenzyl)-*N*-(5-fluoro-2-phenoxyphenyl)acetamide (DAA1106) (Scheme 1) has been reported as a potent and selective ligand for PBR.[8,9] DAA1106 displayed a high affinity for PBR in mitochondrial fractions of rat ($K_i = 0.043$ nM) and monkey ($K_i = 0.188$ nM) brains.[8] Moreover, DAA1106 showed weak affinities ($IC_{50} = 10{,}000$ nM) for melanin, $Kappa_1$ and $GABA_A$ receptors, and negligible affinities ($IC_{50} > 10{,}000$ nM) for 54 others including receptors, ion channels, uptake/transporter and second messenger.[9] To develop a PET tracer that would provide selective imaging of PBR in vivo, and to elucidate the pharmacological role of PBR in the brain, we have labeled DAA1106 by reacting the corresponding desmethyl precursor *N*-(5-fluoro-2-phenoxyphenyl)-*N*-(2-hydroxy-5-methoxybenzyl)acetamide (DAA1123) with [^{11}C]CH_3I[10] in an excellent radiochemical yield as shown in Scheme 1. Moreover, we have determined a high specific binding of [^{11}C]DAA1106 to PBR in the mouse brain. Now, [^{11}C]DAA1106 is being used for investigating PBR in the human brain.

*Corresponding author. Tel.: +81-43-206-4041; fax: +81-43-206-3261; e-mail: zhang@nirs.go.jp

0960-894X/03/$ - see front matter © 2002 Elsevier Science Ltd. All rights reserved.
PII: S0960-894X(02)00886-7

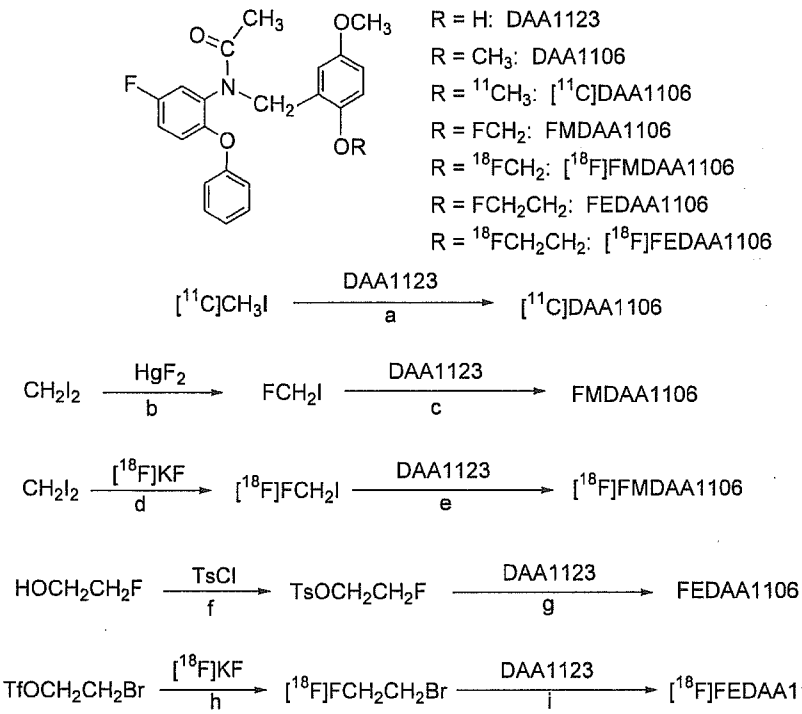

Scheme 1. Structures, chemical synthesis and radiosynthesis: (a) NaH, DMF, 30 °C, 5 min, 81%; (b) 60 °C, 80–100 mm Hg, 10 h, 15%; (c) NaH, DMF, 0 °C, 1 h, 78%; (d) 100 °C, 10 min, 8%; (e) NaH, DMF, 15 °C, 10 min, 86%; (f) pyridine, 25 °C, 4 h, 48%; (g) NaH, DMF, 25 °C, 8 h, 37%; (h) *o*-dichlorobenzene, 130 °C, 5 min, 57%; (i) NaH, DMF, 130 °C, 10 min, 29%.

This success prompted us to design two ^{18}F-labeled analogues of [^{11}C]DAA1106: *N*-(5-fluoro-2-phenoxyphenyl)-*N*-(2-[^{18}F]fluoromethyl-5-methoxybenzyl)acetamide ([^{18}F]-FMDAA1106) and *N*-(5-fluoro-2-phenoxyphenyl)-*N*-(2-[^{18}F]fluoroethyl-5-methoxybenzyl)acetamide ([^{18}F]-FEDAA1106) as putative PET ligands for PBR (Scheme 1). First, because of the molecular similarity and bioisoteric property of *O*–CH_2F and *O*–CH_2CH_2F with *O*–CH_3 group, the two compounds may display similar affinities for PBR with DAA1106. Second, compared with DAA1106, FMDAA1106 and FEDAA1106 were more lipophilic and may readily pass through the blood-brain barrier, which is necessary for a suitable PET tracer over the brain. Third, the [^{18}F]fluoroalkyl substitution may lead to significant improvement in tracer behavior including pharmacokinetics, as can be seen in some examples of PET tracers.[11,12] Finally, since ^{18}F has advantage over ^{11}C, with a longer half-life (110 min vs 20 min) and a lower positron energy (650 KeV vs 960 KeV), ^{18}F is convenient for long-time storage and long-distance transportation and could give a higher quality of images with higher spatial resolution.

In this paper, we report: (1) synthesis, binding affinities of FMDAA1106 and FEDAA1106 to PBR and CBR; (2) radiosynthesis of [^{18}F]FMDAA1106 and [^{18}F]FEDAA1106 and ex vivo autoradiograms of their binding sites in the rat brain.

The non-radioactive FMDAA1106 and FEDAA1106 were prepared according to Scheme 1. The fluoromethylating agent fluoromethyl iodide (FCH_2I) was prepared by reacting diiodomethane (CH_2I_2) with HgF_2 under reduced pressure in a 15% yield.[13] Reaction of DAA1123 with FCH_2I in the presence of NaH at 0 °C was accomplished rapidly to give FMDAA1106[14] in a 78% yield. Reaction of DAA1123 with NaH and 1-fluoro-2-tosyloxyethane (FCH_2CH_2OTs), which was prepared from 2-fluoroethanol and *p*-toluenesulfonyl chloride, gave FEDAA1106[14] in a 75% yield.

[^{18}F]FMDAA1106 and [^{18}F]FEDAA1106 were synthesized as shown in Scheme 1. The labeling intermediate [^{18}F]fluoromethyl iodide ([^{18}F]FCH_2I) or 2-[^{18}F]fluoroethyl bromide ([^{18}F]FCH_2CH_2Br) for the radiosynthesis was prepared by the reaction of [^{18}F]F^- with CH_2I_2 or 2-bromoethyl triflate ($BrCH_2CH_2OTf$) using a newly developed automated system.[15] [^{18}F]FCH_2I or [^{18}F]-FCH_2CH_2Br was purified by distillation and trapped in a solution of DMF containing DAA1123 (1 mg) and NaH (6–8 μL, 0.5 g/20 mL DMF) at −15 °C. After the radioactive reagent trapping ended, the fluoromethylation finished perfectly, whereas the fluoroethylation required a further 10 min at 130 °C. The desired product was purified by HPLC using a reversed phase semi-preparative YMC J'sphere ODS-H80 column (10 mm ID × 250 mm) and a mixture of CH_3CN/H_2O (5.5/4.5 for [^{18}F]FMDAA1106 and 6/4 for [^{18}F]FEDAA1106). Using CAPCELL PAK C_{18} analytic column (4.6 mm ID × 250 mm) and a mixture of CH_3CN/H_2O (7/3), the identity of [^{18}F]FMDAA1106 or [^{18}F]FEDAA1106 was confirmed by co-injecting with the corresponding non-radioactive sample. The retention time was 6.1 min for [^{18}F]FMDAA1106 and 6.3 min for [^{18}F]FEDAA1106 at a flow rate of 2 mL/min, respectively. In the final product solution, no significant DAA1123 peak was determined by HPLC. The radiochemical purity of [^{18}F]FMDAA1106 or [^{18}F]FEDAA1106 was higher

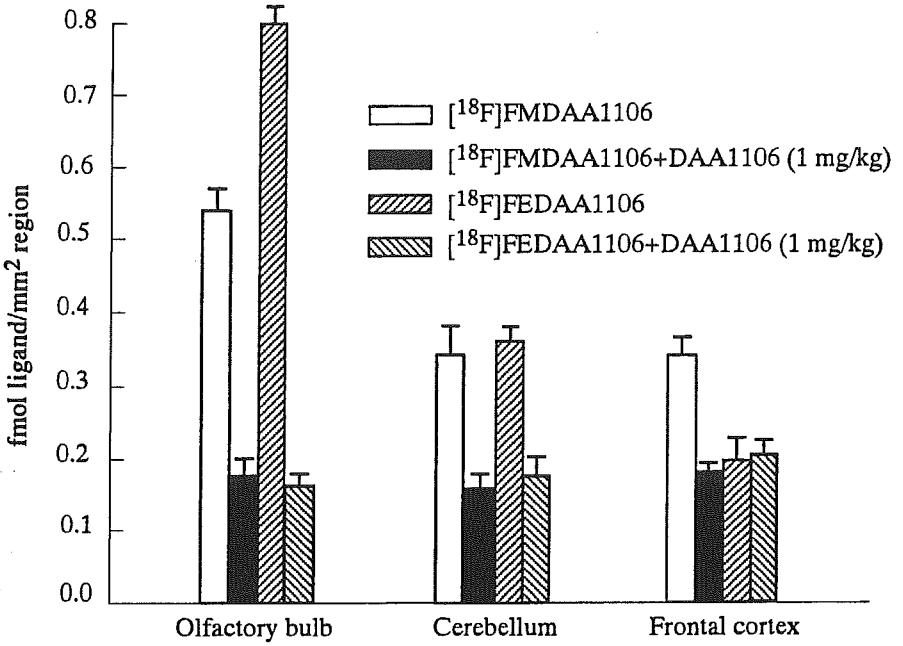

Figure 1. Ex vivo autoradiographic localizations or [^{18}F]FMDAA1106 and [^{18}F]FEDAA1106 in the rat brains at 30 min postinjection (20 MBq, 0.1 nmol). Quantified values (fmol/mm^2) of the ex vivo bindings in the olfactory bulb, cerebellum and frontal cortex ($n = 8$) were calculated by the method.[16,17]

than 98% and the specific activity was > 120 GBq/μmol as determined from the mass measured from the HPLC UV analysis. The radiochemical purities of two radioligands remained > 95% after maintenance of the preparations at 25 °C for 4 h, and they were stable for performing evaluation.

The in vitro binding (IC_{50}) studies of FMDAA1106 and FEDAA1106 to PBR were performed using [^{11}C]DAA1106 according to the previous method.[16,17] As shown in Table 1, FEDAA1106 displayed 2-fold higher affinity for PBR than DAA1106, whereas FMDAA1106 displayed similar affinity with DAA1106. This result showed that substituting O–CH_3 group with O–CH_2CH_2F group augmented the binding affinity, whereas substituting with O–CH_2F group did not obviously affect the affinity for PBR. FEDAA1106 was 10-fold more potent than PK11195, the most commonly used ligand for PBR. Competition binding site analyses were also used to evaluate the comparative affinities of FMDAA1106 and FEDAA1106 for CBR labeled by [^{11}C]flumazenil (a selective CBR ligand) (Table 1). The IC_{50} values of FEDAA1106 and FMDAA1106 for CBR in the rat brain were > 10 μM, 10^4-fold lower than for PBR. These findings revealed that FEDAA1106 and FMDAA1106 exhibited high potency for PBR and negligible affinities for CBR. The distribution coefficients (log Ps) of [^{18}F]FMDAA1106 and [^{18}F]FEDAA1106 were determined in the water/octanol system at pH 7.4 using the shaking method according to the previous procedure[18] (Table 1).

Table 1. In vitro binding affinity (IC_{50}) for PBR and CBR, and octanol/water distribution coefficient (log P)

Ligand	IC_{50} (nM)[a]		Log P
	[^{11}C]DAA1106 displacement (PBR)	[^{11}C]Flumazenil displacement (CBR)	
FMDAA1106	1.71	> 10,000	3.70
FEDAA1106	0.77	> 10,000	3.81
DAA1106	1.62	> 10,000	3.65
PK11195	8.26	> 10,000	No test

[a]IC_{50} was obtained from 9 concentrations of compound using at least 8 slices of rat brains ($n = 3$).

Figures 1 and 2 show ex vivo autoradiographic localizations of [^{18}F]FMDAA1106 and [^{18}F]FEDAA1106 binding sites in the rat brains at 30 min postinjection. As can be seen in comparison with the sagittal sections of the control rat brain (Figs. 1 and 2a and b), both of these radioligands showed a considerably high brain uptake, indicating that they can pass through the blood-brain barrier, which is a prerequisite for a promising PET tracer. This finding was compatible with their

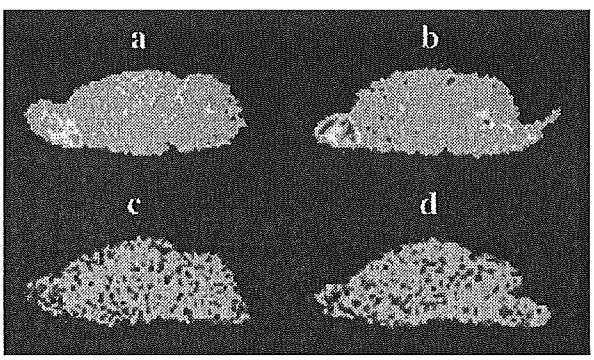

Figure 2. Ex vivo autoradiogram of [^{18}F]FMDAA1106 and [^{18}F]FEDAA1106 in the sagittal sections of rat brains at 30 min postinjection (20 MBq, 0.1 nmol): (a) [^{18}F]FMDAA1106; (b) [^{18}F]FEDAA1106; (c) [^{18}F]FMDAA1106 + DAA1106 (1 mg/kg), (d) [^{18}F]FEDAA1106 + DAA1106 (1 mg/kg).

lipophilicities as shown in Table 1. A significantly-high radioactivity was observed in the olfactory bulb, the high PBR density area in the rat brain.[8,19] Followed by the olfactory bulb, a moderate radioactivity level was observed in the cerebellum, whereas a low uptake was seen in the other brain regions such as frontal cortex. The uptake pattern of radioactivity was not only consistent with [^{3}H]DAA1106 and [^{3}H]PK11195 binding sites in the rat brain,[8,19] but was also in accordance with the regional distribution of PBR in the brain.[1–3] The ratio of radioactivity in the olfactory bulb to that in the frontal cortex was 3.5 for [^{18}F]FEDAA1106 and 1.6 for [^{18}F]-FMDAA1106. The difference between the radioactivity distributions of the two tracers in the olfactory bulb and frontal cortex may be due to their stabilities in the rat brain. Metabolite analysis for the brain homogenate displayed that [^{18}F]FEDAA1106 was not metabolized, whereas [^{18}F]FEDAA1106 was decomposed in the brain at 30 min postinjection. Co-injection with non-radioactive DAA1106 (1 mg/kg) exhibited a significant reduction of [^{18}F]FMDAA1106 or [^{18}F]FEDAA1106 concentration in the brain regions when compared with the control groups (Figs. 1 and 2c and d). As for [^{18}F]FMDAA1106, the radioactivity levels were reduced to 30–50% of control in the brain regions including the olfactory bulb. As for [^{18}F]FEDAA1106, the most significantly reduced uptake (less than 20% of control) was found in the olfactory bulb, whereas a modest decrease (40–60%) was observed in the other regions. These findings revealed that [^{18}F] FMDAA1106 and [^{18}F]FEDAA1106 displayed high specific bindings in the rat brain, especially in the olfactory bulb. Since FMDAA1106 and FEDAA1106 had potent affinities for PBR, these radioligands may have high binding sites to PBR in the rat brain.

In conclusion, [^{18}F]FMDAA1106 and [^{18}F]FEDA-A1106 were designed, synthesized and evaluated as two potent radioligands for PBR. They showed high specific bindings to PBR in the rat brain and may become promising PET tracers for PBR. Further investigation into the binding of [^{18}F]FMDAA1106 and [^{18}F]FEDAA1106 to PBR in the primate brains is currently underway.

Acknowledgements

The authors are grateful to Dr. A. Nakazoto (Taisho Pharmaceutical Co., Ltd.) for giving us the samples (DAA1123 and DAA1106) and helpful suggestions. We also thank the crew of the Cyclotron Operation Section and Radiopharmaceutical Chemistry Section of National Institute of Radiological Sciences (NIRS) for their support in the operation of the cyclotron and production of radioisotopes.

References and Notes

1. Anholt, R. R. H.; DeSouza, E. B.; Oster-Granite, M. L.; Synder, S. H. *J. Pharmac. Exp. Ther.* **1985**, *233*, 517.
2. Gavisg, M.; Katz, Y.; Bar-Ami, S.; Wizman, R. *J. Neurochem.* **1992**, *58*, 1589.
3. Zisterer, D. M.; Williams, D. C. *Gen. Pharmac.* **1997**, *29*, 305.
4. Papadopoulos, V.; Amri, H.; Li, H.; Yao, Z.; Brown, R. C.; Vidic, B.; Culty, M. *J. Pharmacol. Exp. Ther.* **2001**, *299*, 793.
5. Wieland, S.; Belluzzi, J.; Stein, L.; Lan, N.-C. *Psychopharmacology* **1995**, *118*, 65.
6. Pappata, S.; Levasseur, M.; Gunn, R. N.; Myers, R.; Crouzel, C.; Syrota, A.; Jones, T.; Kreutzberg, G. W.; Banati, R. B. *Neurology* **2000**, *55*, 1052.
7. Sauvageau, A.; Desjardins, P.; Lozeva, V.; Rose, C.; Hazell, A. S.; Bouthillier, A.; Butterwort, R. F. *Metab. Brain. Dis.* **2002**, *17*, 3.
8. Chaki, S.; Funakoshi, T.; Yoshikawa, R.; Okuyama, S.; Okubo, T.; Nakazoto, A.; Nagamine, M.; Tomisawa, K. *Eur. J. Pharmacol.* **1999**, *371*, 197.
9. Okuyama, S.; Chaki, S.; Yoshikawa, R.; Ogawa, S.; Suzuki, Y.; Okubo, T.; Nakazato, A.; Nagamine, M.; Tomisawa, K. *Life Sci.* **1999**, *64*, 1455.
10. Suzuki, K.; Inoue, O.; Hashimoto, K.; Yamasaki, T.; Kuchiki, M.; Tamate, K. *Appl. Radiat. Isot.* **1985**, *36*, 971.
11. Chi, D.-Y.; Kilbourn, M. R.; Katzenellenbogen, J. A.; Brodack, J. W.; Welch, M. J. *Appl. Radiat. Isot.* **1986**, *37*, 1173.
12. Mach, R. H.; Ehrenkaufer, R. L. E.; Greenberg, J. H.; Shao, L.-X.; Morton, T. E.; Evora, P. H.; Nowak, P. A.; Luedtke, R. R.; Cohen, D.; Reivich, M. *Synapse* **1995**, *19*, 177.
13. Zheng, L.; Berridge, M. S. *Appl. Radiat. Isot.* **2000**, *52*, 55.
14. FMDAA1106: white powder; mp: 71–72 °C; IR (Nujol): 1680 cm^{-1}; ^{1}H NMR (200 MHz, $CDCl_3$) δ: 7.18–7.40 (2H, m), 6.71–7.13 (8H, m), 6.28–6.44 (1H, m), 5.30 (1H, d, J = 49 Hz), 4.71 (2H, dd, J = 7, 46 Hz), 3.71 (3H, s), 2.12 (3H, s); FABMS (m/z): 414.2 ($M^+ + 1$). Anal. ($C_{23}H_{21}F_2NO_4$) C, H, N. FEDAA1106: white powder; mp: 54–56 °C; IR (Nujol): 1685 cm^{-1}; ^{1}H NMR (200 MHz, $CDCl_3$) δ: 7.26–7.59 (2H, m), 6.22–7.19 (9H, m), 4.88 (2H, dt, J = 4, 41 Hz), 4.65 (2H, dd, J = 7, 46 Hz), 4.12 (2H, dt, J = 4, 27 Hz), 3.80 (3H, s), 2.15 (3H, s); FABMS (m/z): 427.2 ($M^+ + 1$). Anal. ($C_{24}H_{23}F_2NO_4$) C, H, N.
15. Zhang, M.-R.; Tsuchiyama, A.; Haradahira, T.; Yoshida, Y.; Furutsuka, K.; Suzuki, K. *Appl. Radiat. Isot.* **2002**, *9*, 335.
16. Sihver, S.; Sihver, W.; Bergstrom, M.; Hoglund, U.; Sjoberg, P.; Langstrom, B.; Watanabe, Y. *J. Pharmacol. Exp. Ther.* **1999**, *290*, 917.
17. Zhang, M.-R.; Haradahira, T.; Maeda, J.; Okauchi, T.; Kawabe, K.; Kida, T.; Obayashi, S.; Suzuki, K.; Suhara, T. *Nucl. Med. Biol.* **2002**, *29*, 469.
18. Zhang, M.-R.; Tsuchiyama, A.; Haradahira, T.; Furutsuka, K.; Yoshida, Y.; Kida, T.; Noguchi, J.; Irie, T.; Suzuki, K. *Nucl. Med. Biol.* **2002**, *29*, 463.
19. Funakoshi, T.; Chaki, S.; Okuyama, S.; Okubo, T.; Nakazato, A.; Nagamine, M.; Tomisawa, K. *Res. Commun. Mol. Pathol. Pharmacol.* **1999**, *105*, 35.

ELSEVIER

Nuclear Medicine and Biology 30 (2003) 779–784

NUCLEAR MEDICINE — AND — BIOLOGY

www.elsevier.com/locate/nucmedbio

Metabolite analysis of [^{11}C]Ro15-4513 in mice, rats, monkeys and humans

T. Kida[a,b], J. Noguchi[a,b], M.-R. Zhang[a,b], T. Suhara[c], K. Suzuki[a,*]

[a]*Department of Medical Imaging, National Institute of Radiological Sciences, Chiba 263-8555 Japan*
[b]*SHI Accelerator Service, Tokyo 141-8686 Japan*
[c]*Brain Imaging Project, National Institute of Radiological Sciences, Chiba 263-8555 Japan*

Abstract

We performed in vitro and in vivo assays of the metabolism of [^{11}C]Ro15-4513 over time in the plasma of mice, rats, monkeys and humans, using a radio-HPLC equipped with a sensitive positron detector, in order to compare the metabolic rates of the radiopharmaceutical agent among the different animal species and to establish a highly sensitive analytical method for the radiotracer agent. We also examined the metabolism of [^{11}C]Ro15-4513 in the brain tissue of mice and rats.

The analytical method used in this study permitted detection of even extremely low levels of radioactivity (approximately 5,000 dpm). In vitro experiments revealed that [^{11}C]Ro15-4513 in the blood was metabolized to hydrolysate [^{11}C]A. The species were classified in descending order of the metabolic rate of the radiotracer in vitro as follows; mice, rats, and monkeys/humans. In the in vitro experiment, the percentage of the unchanged drug in the plasma at 60 minutes postdose was 9% in mice, 70% in rats, 97% in monkeys, and 98% in humans. In vivo metabolite analysis in the blood showed the presence of two radioactive metabolites, consisting of one hydrolysate [^{11}C]A and another unidentified substance. The species were classified in descending order of the metabolic rate of the radiotracer in vivo as follows; mice, rats/humans, and monkeys. The percentage of the unchanged drug in the plasma was 6% in mice, 21% in rats, 26% in humans, and 40% in monkeys. Furthermore, the in vitro and in vivo experiments conducted to analyze the metabolism of [^{11}C]Ro15-4513 in the brain tissue of mice and rats revealed that the radiotracer was metabolized to some extent in the brain tissue of these animals. In the in vivo experiment, the percentage of the unchanged drug at 60 min postdose was 86% in the brain tissue of mice and 88% in the brain tissue of rats, while in the in vitro experiment, the corresponding percentage was 93% in mice, and 91% in rats.

Keywords: [^{11}C]Ro15-4513; Metabolite analysis; PET

1. Introduction

Positron emission tomography (PET) is a non-invasive technique used in the field of nuclear medicine for displaying and quantitatively measuring bio-function in a living subject using biologically relevant compounds labeled with positron-emitting radionuclides. PET plays an important role in the diagnosis and investigation of psychiatric disorders, such as depression and schizophrenia, since it allows one to determine the density of neurotransmitter receptors and their occupancy in the brain. Although PET allows visualization of the distribution of radiolabeled compounds and the changes in their concentration over time, it provides no information about the chemical degradation of the drug itself. When a radiolabeled compound that is rapidly metabolized after injection is used in PET, its metabolites may affect the acquisition of data. Therefore, it is very important in a PET study to examine the chemical forms of the metabolites of the radiolabeling pharmaceutical drugs in the plasma and the brain. The metabolism of this tracer in plasma has been investigated with radio-TLC and radio-HPLC, or other methods [9,10]. However, radio-HPLC has been widely used because the high sensitivity due to a large sample load, the high resolution, and real-time monitoring by connecting the HPLC outlet to multiple detectors arranged in series.

Metabolite analysis of a radiotracer usually consists of the following procedures: 1) blood sample collection at regular intervals and assessment of radioactivity, 2) separation of plasma by centrifugation and measurement of radio-

* Corresponding author. Tel.: +81-43-206-3262; fax: +81-43-206-3261.
E-mail address: kazutosi@nirs.go.jp (K. Suzuki).

0969-8051/03/$ – see front matter
doi:10.1016/S0969-8051(03)00059-3

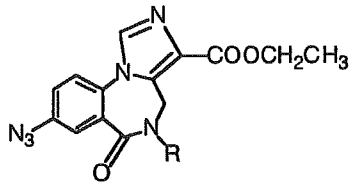

R = H: Ro 44-3902
R = CH_3: Ro 15-4513
R = $^{11}CH_3$: [^{11}C]Ro15-4513

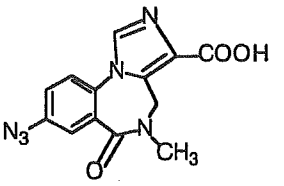

A

Scheme 1. Structures of Ro15-4513 and its analogs.

activity, and 3) radio-HPLC analysis to determine the percentage of the unchanged drug following plasma deproteination [6,9,15]. Tracers labeled with short-lived radionyclides, such as ^{11}C ($t_{1/2}$ = 20 min), ^{13}N ($t_{1/2}$ = 10 min), and ^{18}F ($t_{1/2}$ = 110 min), decay with positron emission over time. Besides, the radioactivity of the compound is dilured in the plasma as a result of its distribution into tissues, metabolism, and excretion. Therefore, metabolite analysis of radiopharmaceuticals for PET studies necessitates establishment of a highly sensitive assay for radioactivity, as well as establishment of a quick blood processing system and analytical method [9]. Recently, Takei et al. developed a sensitive positron detector for HPLC [17]. They indicated that this sensitive positron detector could detect the metabolites of [^{11}C]FLB-457, a dopamine D-2 ligand, in blood samples (3,900 dpm) of mice, even at 90 minutes after injection of 10 MBq of the radiotracer.

Ro15-4513 (Ethyl 8-azido-5, 6-dihydro-5-methyl-6-oxo-4H-imidazo[1,5-a] [1,4] benzodiazepine-3-carboxylate, Scheme 1), an azide derivative of flumazenil, is a partial inverse agonist of the central benzodiazepine receptor (BZ-R) [11]. BZ-R forms a complex with $GABA_A$ ($GABA_A$/BZ-R complex). This complex is known to be involved in the induction of anxiety, convulsions, and hypnosis through Cl^-. Ro15-4513 labeled with ^3H or ^{11}C has been demonstrated to strongly bind to the $GABA_A$/BZ-R complex in vitro [2,14,18]. Clinical PET studies have demonstrated uptake of [^{11}C]Ro15-4513 in the limbic system (cingulate gyrus, insula and hippocampus) where BZ-R is expressed in abundance. [^{11}C]Ro15-4513 has been shown to be highly useful in mental disorder research [8,13]. [^{11}C]Flumazenil, a BZ-R ligand, was reported to be rapidly metabolized in the plasma of humans [9], but few data are available on the metabolism of [^{11}C]Ro15-4513, an analog of flumazenil. We conducted this study to establish a highly sensitive assay system for detecting the metabolites of [^{11}C]Ro15-4513, in order to perform highly accurate clinical PET studies using a radio-HPLC equipped with a sensitive positron detector developed by Takei et al. [17]. Changes in [^{11}C]Ro15-4513 were quantified over time in mice, rats, monkeys, and humans, and the metabolic rate of the radiotracer was compared among the species. Furthermore, in vivo and in vitro assays of the metabolites of [^{11}C]Ro15-4513 in the brain tissue were conducted in mice and rats.

2. Materials and Methods

2.1. Radiosynthesis of [^{11}C]Ro15-4513

Ro15-4513 and desmethyl Ro15-4513 (Ro44-3902, Scheme 1) were kindly provided by Roche (Basel, Switzerland). Carbon-11 (^{11}C) was produced by the $^{14}N(p, \alpha)\ ^{11}C$ nuclear reaction using a CYPRIS HM-18 cyclotron (Sumitomo Heavy Industry, Tokyo, Japan).

[^{11}C]Ro15-4513 was synthesized by N-methylation of Ro44-3902 with [^{11}C]methyl iodide in the presence of NaH [7]. The radiochemical purity and specific activity of [^{11}C]Ro15-4513 for the metabolite analysis were >95% and 30 – 290 GBq/μmol, respectively (at the end of the synthesis).

2.2. Synthesis of 8-azido-5,6-dihydro-6-oxo-4H-imidazo[1,5-a] [1,4]benzodiazepine-3-carboxylic acid (A)

Scheme 1 shows the structure formulas of parent and the identified metabolites. A mixture of Ro15-4513 (10 mg) and 1N-NaOH (1 mL) in EtOH (2 mL) was stirred for 15 min at room temperature. The reaction mixture was neutralized with 1N HCl and injected onto a semi-preparative column (Megapak C_{18}, 10 mm ID × 250 mm) set to the JASCO HPLC system. The column was eluted with CH_3CN/H_2O (225/275) at a flow rate of 6.0 mL/min, and a UV (254 nm) fraction having a retention time of 2.3 min was collected. Removal of the solvents under reduced pressure gave the hydrolysis product A as a white solid (Scheme 1). mp: 201–203°C (uncorrected). ^{1}H-NMR (300 Hz, DMSO-d_6 + $CDCl_3$) δ: 7.24 (1H, s), 6.77 (1H, d, J = 9.0 Hz), 6.68 (1H, d, J = 2.7 Hz), 6.43 (1H, dd, J = 9.0, 2.7 Hz), 2.38 (2H, s), 2.27 (3H, s). IR (Nujol): 3100, 1690 cm^{-1}. FAB–MS (m/z) calcd for $C_{15}H_{14}N_6O_3$ (M^++1): 299; Found: 299. This sample was used to identify the metabolites of [^{11}C]Ro15-4513.

2.3. Metabolite analysis

The study of [^{11}C]Ro15-4513 metabolism in humans was approved by the Ethics and Radiation Safety Committee of the National Institute of Radiological Sciences. Blood samples were obtained from 19 normal human volunteers (ranging in age from 21-31 years old). The study in mice, rats and monkeys was carried out according to the recommendations of the Committee for the Care and Use of Laboratory Animals, National Institute of Radiological Sciences. A young male rhesus monkey (macaca mulatta) weighing about 5 kg (3 years old) was anesthetized by repeated injections of ketamine (Ketalar®, 10 mg/kg/h, im). The rats (200 g, male) and mice (30 g, male) used in the study were anesthetized with ether.

The metabolite analysis was carried out using an HPLC analysis system. The system consisted of: a PU610 pump (GL sciences, Tokyo), a Rheodyne injector 7010, a μBondapak C-18 column 7.8 × 300 mm, 10 μm (Waters, Massachusetts) Waters μBondapak C-18 guard column, and a UV620-spectrophotometer 254 nm (GL science, Tokyo) equipped with a sensitive positron detector [16] Phosphoric acid (6 mM)/CH_3CN (1:1) was used as the mobile phase at a flow rate of 2.5 mL/min. The injection volume loaded on the HPLC column was 10 μL-1 mL. The retention time (t_R) for [^{11}C]A was 6.2 min, whereas that for [^{11}C]Ro15-4513 was 8.5 min.

2.3.1. Blood

a) In vivo

After intravenous administration of Ro15-4513 to the human volunteers (280 ± 100 MBq), monkeys (160 ± 60 MBq), rats (65 ± 25 MBq) and mice (80 ± 35 MBq), blood samples (0.5-1.5 mL) were obtained from the human volunteers at 2, 4, 9, 14, 19, 39 and 59 min, from the monkeys at 1, 5, 10, 30 and 60 min, and from the mice and rats at 1, 3, 5, 10, 30 and 60 min postinjection. The blood samples were centrifuged at 15000 rpm in a KUBOTA centrifuger (3615 model) for 1 min at 4°C, to separate plasma. The plasma specimens (0.2-0.7 mL) were then collected in test tubes containing the same volume of CH_3CN. After the tubes were vortexed for 15 sec and centrifuged at 15000 g for 1 min for deproteination, the supernatants (0.3-1.2 mL) were collected. The radioactivity in the supernatants (0.3-1.2 mL) and in the residual precipitates after centrifugation was measured in an A5530 gamma counter (PACKARD instrument, Tokyo, Japan). Then, the supernatants (0.3-1 mL) were mixed with standard Ro15-4513 (50 μg/mL, 10 μL) and the hydrolysis product A (100 μg/mL, 10 μL) injected into the HPLC column for analysis under the conditions described above.

b) In vitro

[^{11}C]Ro15-4513 (3 MBq, specific activity: 110 ± 25 GBq/μmol) was added to blood samples (1 mL) obtained from human volunteers (n = 3, 29-35 years old), monkeys (n = 1, 3 years old), rats (n = 3, 10 weeks old), and mice (n = 3, 11 weeks old). The radioactive mixtures containing the mouse, rat and monkey blood samples were allowed to stand for 1, 5, 10, 30 and 60 min, while those containing the human blood samples were allowed to stand for 5 and 30 min. To determine the effect of temperature on the rate of metabolism, the mouse blood samples were mixed with [^{11}C]Ro15-4513 and placed in an ice-bath for 10 min. As control, saline mixed with [^{11}C]Ro15-4513 (3 MBq, specific activity: 110 GBq/μmol) was incubated at room temperature for 60 min. At the end of the incubation periods, the samples were respectively loaded on the HPLC column and analyzed under the conditions described above.

2.3.2. Brain

a) In vivo

After intravenous administration of [^{11}C]Ro15-4513 (74-80 MBq/200 μL) into mice (n = 3) and rats (n = 3), the animals were sacrificed by cervical dislocation at 1, 5, 15, 30 or 60 min postinjection.

The cerebral cortex and hippocampus were dissected from the brain and homogenized in 0.5 mL of distilled water. After adding CH_3CN (0.9 mL) to the homogenate, the mixture was centrifuged at 15000 g for 1 min, and the supernatant was collected. The radioactive mixture containing the standard solution A (the hydrolysis product of Ro15-4513) and Ro15-4513 was treated as described above.

b) In vitro

The cerebral cortex and hippocampus were quickly removed from the rats and mice and homogenized in 0.5 mL of distilled water. The radioactive mixtures were incubated at room temperature for 60 min. After adding CH_3CN (0.9 mL) to the homogenate, the mixture was centrifuged at 15000 g for 1 min, and the supernatant was collected. The radioactive sample containing the standard solution A was treated as described above.

3. Results and Discussion

We conducted this study with the aim of establishing an accurate method for analyzing the metabolites of [^{11}C]Ro15-4513 in the blood of mice, rats, monkeys and humans, and in the brain tissue of rats and mice, in PET studies using the radiotracer. The radio-HPLC equipped with the highly sensitive positron detector developed by Takei et al. [16] enabled us to detect [^{11}C]Ro15-4513 and its metabolites in blood samples (approximately 5,000 dpm) even after 60 minutes of injection of the radiotracer at a dose of 185 MBq. Plasma deproteination with acetonitrile allowed us to recover 93.6 ± 2.0% of radioactivity from the supernatant of the blood specimens. A mixture of physiological saline and [^{11}C]Ro15-4513 at the purity of 99.0% was analyzed as the control, and the radioactivity recovery rate was 98.9%. The good radioactivity recovery rate and negligible degradation of the radiotracer may be indicative

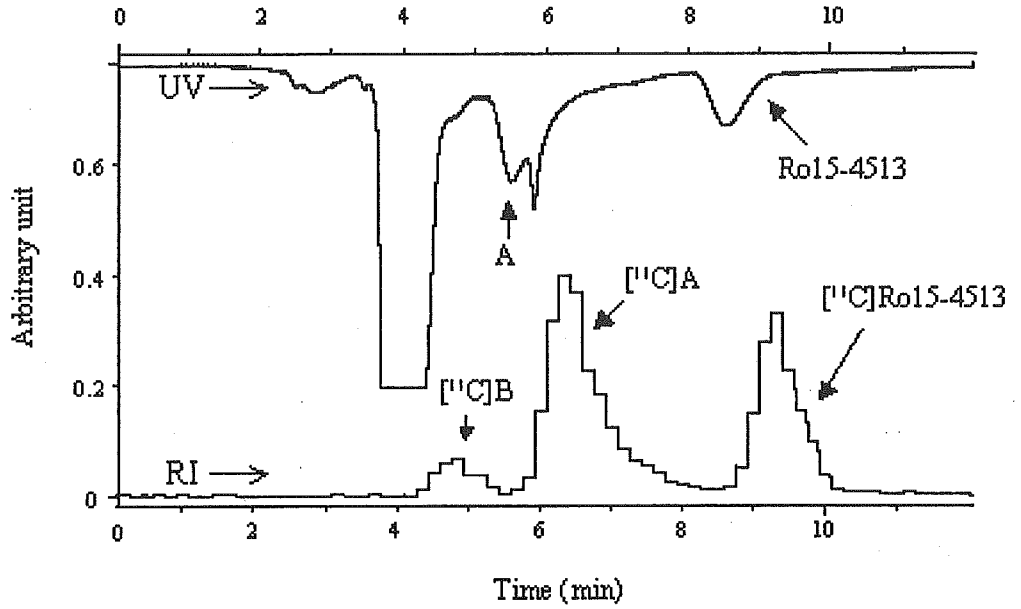

Fig. 1. HPLC analysis of metabolites in the plasma at 14 min after injection of [^{11}C]Ro15-4513 in humans. A and [^{11}C]A: hydrolysates of Ro15-4513 and [^{11}C]Ro15-4513; [^{11}C]B: unknown radioactive metabolite.

of the appropriateness of the deproteination procedure for detection of the unchanged drug in the plasma.

In the case of humans, blood was collected at 14 min after injection of 400 MBq of [^{11}C]Ro15-4513, Ro15-4513 (50 μg/mL, 10 μL) and its hydrolysate A (100 μg/mL, 10 μL) were then added to the collected blood samples.

Fig. 1 shows the results of HPLC analysis of these blood samples, which showed two other radioactive peaks (t_R([^{11}C]B) = 4.4 min, t_R([^{11}C]A) = 6.2 min), besides the peak of [^{11}C]Ro15-4513 (t_R = 8.5 min). The peak of [^{11}C]A was consistent with that of hydrolysate A of Ro15-4513. Esters are known to be hydrolyzed by various esterases. Metabolite analysis of [^{11}C]flumazenil, an analog of [^{11}C]Ro15-4513, has revealed that carboxylic acid is formed when [^{11}C]flumazenil are hydrolyzed [9]. Therefore, we presumed that [^{11}C]A were also formed when [^{11}C]Ro15-4513 were hydrolyzed. The identification of [^{11}C]B was not carried out.

Fig. 2 shows the results of the in vitro [^{11}C]Ro15-4513 metabolite analysis in the blood samples obtained from mice, rats, monkeys and humans. [^{11}C]Ro15-4513 was metabolized to [^{11}C]A alone, while no peak corresponding to [^{11}C]B was found. In vitro, [^{11}C]Ro15-4513 was rapidly metabolized in the plasma of mice and rats during the first 60 minutes after its administration, while the radiotracer was hardly metabolized in that of humans and monkeys. The percentage of the parent drug at 60 min postdose in vitro was 9% in mice, 70% in rats, 97% in monkeys, and 98% in humans. These findings suggest that metabolism of the radiopharmaceutical drug persists in blood samples even after they are collected from the mice and rats. Accordingly, an in vivo metabolite analysis using these rodents must be carefully evaluated. In this study, we employed two methods to inhibit further metabolism of [^{11}C]Ro15-4513 in the blood samples after they were collected. The first was to add 2 N HCl (up to 10 μL) to blood samples immediately after they were collected from the rodents. With this method, the percentage of the unchanged drug was 56.6 ± 1.8%, while that in the control left untreated at room temperature after the collection was 48.2 ± 1.7%. Therefore, the addition of HCl was not considered to be useful for blocking degrada-

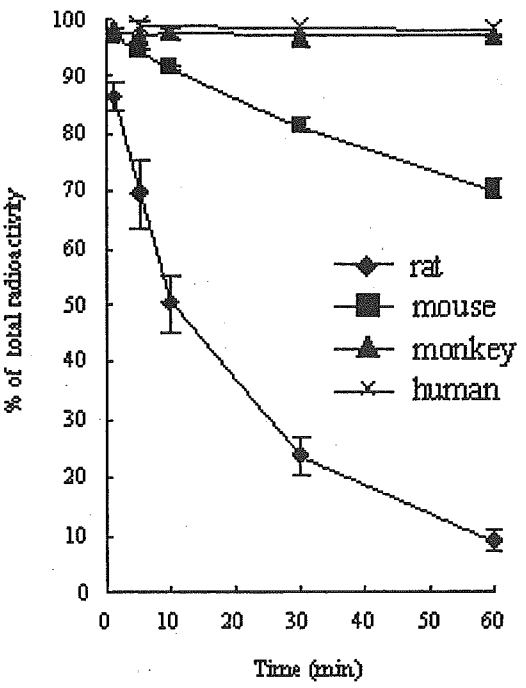

Fig. 2. Metabolism of [^{11}C]Ro15-4513 over time in vitro, in the blood samples of humans, monkeys, rats and mice.

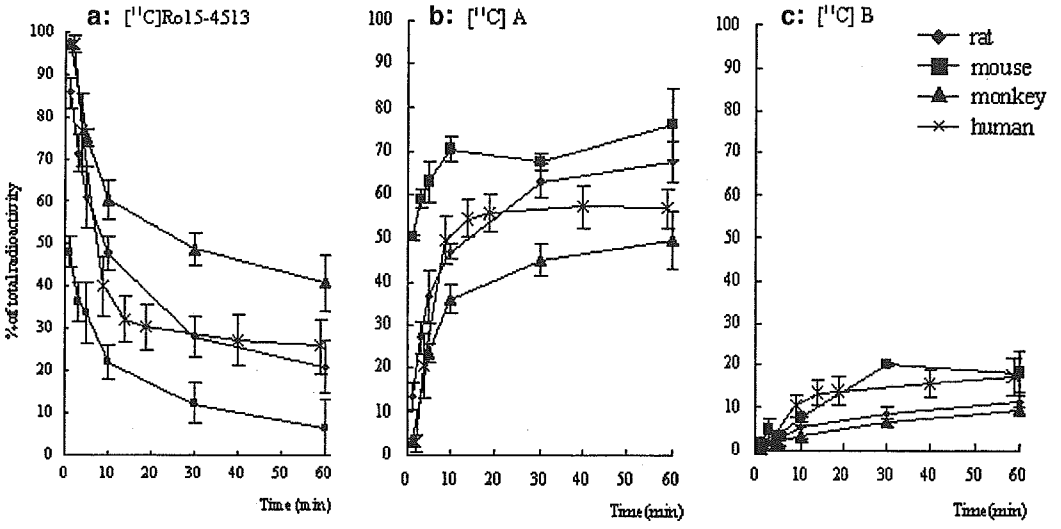

Fig. 3. Metabolism of [^{11}C]Ro15-4513 over time in vivo, in the blood of humans, monkeys, rats and mice. (a) Unchanged [^{11}C]Ro15-4513. (b) Formation of [^{11}C]A (hydrolysate of [^{11}C]Ro15-4513) by metabolism. (c) Formation of the unknown radioactive metabolite [^{11}C]B.

tion of the radiotracer. In the other method, fresh blood specimens collected from rats and mice were placed in an ice bath. In this case, the percentage of the parent drug was 88.5 ± 1.5%. Such good results indicate that the ice bath method may be relatively more helpful for a more accurate assay of the radiotracer. Further studies, however, are required for effecting complete inhibition of the metabolism of [^{11}C]Ro15-4513 in blood specimens after they are collected from rodents. On the other hand, no special procedures may be necessary for blocking the metabolism of [^{11}C]Ro15-4513 in blood samples taken from monkeys and humans, since the radiolabeled drug level in the plasma remained almost unchanged over time in vitro.

Fig. 3 shows the results of the in vivo [^{11}C]Ro15-4513 metabolite assays in the blood samples drawn from mice, rats, monkeys and humans. The percentage of the parent drug rapidly reduced during the first 10 min in all species after the injection, to 60% in monkeys, 48% in rats, 40% in humans, and 22% in mice, 10 min after the injection. After the first 10 min, the parent drug level in the blood slowly decreased and the percentage at 60 min postdose was 40% in monkeys, 26% in humans, 21% in rats, and 6% in mice. Considerable differences in the metabolism of radiotracers between species have been reported for [^{76}Br]BLIS and [^{11}C]methylspiperone [3,4]. The tendency towards a high metabolic rate of the radiotracers during the first 10 min after injection was also observed for [^{11}C]flumazenil, an analog of [^{11}C]Ro15-4513, and [^{11}C]SCH23390, a dopamine D_1-antagonist [9,11].

This study revealed that while [^{11}C]Ro15-4513 was metabolized to [^{11}C]B and [^{11}C]A in vivo, [^{11}C]A was predominant in all the species. The percentages of [^{11}C]A and [^{11}C]B at 60 minutes postdose were 50 to 75% and 20% or less, respectively. The percentage of [^{11}C]A rapidly increased to 55% during the first 15 min after the injection, and remained almost unchanged in humans. In rats and monkeys, the percentage of [^{11}C]A rapidly increased during the first 10 min and continued to increase steadily thereafter. In contrast, the percentage of [^{11}C]B increased to approximately 14% in humans during the first 15 min after the injection, after which it remained almost unchanged at 60 min postdose, and in rats, mice, and monkeys there was a steady and gradual increase, without a sharp increase during the initial phase. Species were classified in descending order of the metabolic speed of [^{11}C]Ro15-4513 in vivo as, mice, humans/rats, and monkeys. In the case of mice and rats, as mentioned above, metabolic changes of the radiotracer in the plasma continued even after the blood samples were drawn from these animals. This may produce an error in the results. In this study, however, blood samples were cooled immediately after they were collected from the test animals, and then centrifuged to obtain plasma specimens, to which CH_3CN was then added. Accordingly, there was probably little room for error in this metabolite analysis.

Table 1 shows the results of the in vitro and in vivo [^{11}C]Ro15-4513 metabolite assays in mice and rat brain tissue at 60 min postdose. [^{11}C]Ro15-4513 was metabolized in the brain tissue in vitro and in vivo in both species, but only to [^{11}C]A in both the animals. The metabolic rate of the

Table 1
Metabolism of [^{11}C]Ro15-4513 in the brains of rats and mice

	in vivo[a]	*in vitro*[b]
	[^{11}C]Ro15-4513 (%)	[^{11}C]Ro15-4513 (%)
Rats	87.5 ± 3.2	93.0 ± 0.8
Mice	85.7 ± 6.9	91.3 ± 2.3
Control[c]	–	98.9

[a] 60 min after i.v. injection.
[b] incubated with homogenized brain tissue for 60 min at room temperature.
[c] incubated with saline solution for 60 min at room temperature.

radiotracer in brain tissue was slower than that in the plasma. The percentage of the parent drug in vivo was 85.7% in mice and 87.5% in rats, while the percentage in vitro was 93.0% in mice and 91.3% in rats. Metabolites of [^{11}C]Ro15-4513 generated in the plasma are considered to have higher hydrophilicity, which makes it difficult for them to pass the blood-brain barrier. These findings indicate that [^{11}C]Ro15-4513 may not be metabolized to any significant degree in the brain of humans.

We conclude that in vitro, [^{11}C]Ro15-4513 in the plasma was hardly metabolized in monkeys and humans, while in mice and rats, the radiotracer in the plasma was rapidly metabolized. In contrast, in vivo, [^{11}C]Ro15-4513 was rapidly metabolized in all the species, especially during the first 10 min after the injection. Species were classified in descending order of the metabolic rate of the radiotracer, as mice, humans/rats, and monkeys.

Furthermore, the analytical findings of [^{11}C]Ro15-4513 metabolites in the brain tissue in mice and rats suggest that PET images in the brain may mostly reflect the behavior of the parent drug, with miner interference by metabolites.

These results may contribute to more accurate data acquisition in PET studies.

Acknowledgments

The authors thank the staff of National Institute of Radiological Sciences for operation of the cyclotron, synthesis of [^{11}C]Ro15-4513 and blood sampling.

References

[1] Barre L, Debruyne D, Abadie P, Moulin M, Baron JC. A comparison of method for the separation of [^{11}C]Ro15-1788 (Flumazenil) from its metabolites in the blood of rabbits, baboons and humans. Int J Radiat Appl Instrum Part A 1991;42:435–439.

[2] Bencsits E, Ebert V, Tretter V, Sieghart W. A significant part of native γ-aminobutyric acid$_A$ receptors cantaining α_4 subunits do not contain γ or σ subunits. J Bio Chem 1999;274:19613–19616.

[3] Coenen HH, Wienhard K, Stocklin G, Laufer P, Hoboldt I, Pawlik G, Heiss WD. PET measurement of D_2 and S_2 receptor binding of 3-N-([2′-^{18}F]-fluoroethyl)spiperone in baboon brain. Eur J Nucl Med 1988;14:80–87.

[4] Coenen HH, Laufer P, Stocklin G, Wienhard K, Pawlik G, Bocher-Schwarz HG, Heiss K. 3-N-2-[^{18}F]-fluoroethyl-spiperone: a novel ligand for cerebral dopamine receptor studies with PET. Life Sci 1987;40:81–88.

[5] Hall H, Litton J-E, Halldin C, Kopp J. Studies on the binding of [^{3}H]flumazenil and [^{3}H]sarmazenil in post mortem human brain. Hum Psychopharmacology 1992;7:367–377.

[6] Halldin C, Farde L, Högberg T, Mohell N, Hall H, Suhara T, Karlsson P, Nakashima Y, Swah CG. Carbon-11-FLB457: A radioligand for extrastriatal D2 dopamine receptors. J Nucl Med 1995;36:1275–1281.

[7] Halldin C, Farde L, Litton J-E, Hall H, Sedvall G. [^{11}C]Ro15-4513, a ligand for visualization of benzodiazepine receptor binding. Psychopharmacology 1992;108:16–22.

[8] Inoue O, Suhara T, Itoh T, Kobayashi K, Suzuki K, Tateno Y. In vivo binding of [^{11}C]Ro15-4513 in human brain measured with PET. Neurosci Lett 1992;145:133–136.

[9] Ishiwata K, Itou T, Ohyama M, Yamada T, Mishima M, Ishii K, Nariai T, Sasaki T, Oda K, Toyama H, Senda M. Metabolite analysis of [^{11}C]flumazenil in human plasma: assessment as the standardized value for quantitative PET studies. Ann Nucl Med 1998;12:55–59.

[10] Irie T, Fukushi K, Namba H, Iyo M, Tamagami H, Nagatsuka S, Ikota N. Brain acetylcholinesterase activity: validation of a PET Tracer in a rat model of Alzheimer's disease. J Nucl Med 1996;37:649–655.

[11] Nakano T, Satoh T, Mori K, Inoue O. Imaging of the super high affinity binding sites for [^{3}H]Ro15-4513 in rat hippocampus: comparison between in vitro and in vivo binding. Neurosci Lett 1998; 250:161–164.

[12] Pritchett DB, Seeburg PH. γ-Aminobutyric acid$_A$ receptor α_5-subunit creates novel type II benzodiazepine receptor pharmacology. J Neurochem 1990;54:1802–1804.

[13] Suhara T, Inoue O, Kobayashi K, Suzuki K, Itoh T, Tateno Y. No age-related changes in human benzodiazepine receptor binding measured by PET with [^{11}C]Ro15-4513. Neurosci Lett 1993;159:207–210.

[14] Sur C, Farrar SJ, Kerby J, Whiting PJ, Atack JR, Mckernan RM. Preferential coassembly of α4 and s subunits of the γ-aminobutyric acid$_A$ receptor in rat thalamus. Molecular Pharmacology 1999;56: 110–115.

[15] Swahn CG, Halldin C, Farde L, Sedvall G. Metabolism of the PET ligand [^{11}C]SCH23390 identification of two radiolabelled metabolites with HPLC. Hum Psychopharmacology 1994;9:25–31.

[16] Suzuki K, Inoue O, Hashimoto K, Yamasaki T, Kuchiki M, Tamate K. Computer controlled large scale production of high specific activity [^{11}C]Ro15-1788 for PET studies of benzodiazepine receptors. Int J Appl Radiat Isot 1985;36:971–976.

[17] Takei M, Kida T, Suzuki K. Sensitive measurement of positron emitters eluted from HPLC. Appl Radia Iso 2001;55:229–234.

[18] Wong G, Skolnick P. High affinity ligands for 'diazepam-insensitive' benzodiazepine receptors. Eur J Pharmaco-Molecular Pharmacology Section 1992;225:63–68.